A BROADBAND QUADRUPLE-RIDGED WAVEGUIDE RADIATOR

Fan King, et al

Army Missile Research, Development and Engineering Laboratory

Prepared for:

Boeing Aerospace Company

30 June 1974

UNCLASSIFIED

SECURITY CLASSIFICATION OF THIS PAGE (When Data Entered)

REPORT DOCUMENTATION PAGE		READ INSTRUCTIONS BEFORE COMPLETING FORM
1. REPORT NUMBER RE-74-7	2 GOVT ACCESSION NO.	3. RECIPIENT'S CATALOG NUMBER
4. TITLE (and Subtitle) A BROADBAND QUADRUPLE-RIDGED WAVEGUIDE RADIATOR		5. TYPE OF REPORT & PERIOD COVERED Technical Report 6 PERFORMING ORG. REPORT NUMBER RE-74-7
7. AUTHOR(s) Fan King, James S. Yee, Donald R. Erbach		8. CONTRACT OR GRANT NUMBER(s)
9. PERFORMING ORGANIZATION NAME AND ADDRESS US Army Missile Research, Development and Engineering Laboratory US Army Missile Command Redstone Arsenal, Alabama 35809		10. PROGRAM ELEMENT, PROJECT, TASK AREA & WORK UNIT NUMBERS (DA) 1M362303A214 AMCMS Code 632303.11.21401
11 CONTROLLING OFFICE NAME AND ADDRESS		12 REPORT DATE 30 June 1974 13. NUMBER OF PAGES 60
14 MONITORING AGENCY NAME & ADDRESS(if different from Controlling Office)		15 SECURITY CLASS. (of this report) UNCLASSIFIED 15a. DECLASSIFICATION/DOWNGRADING SCHEDULE
16. DISTRIBUTION STATEMENT (of this Report) Approved for public release; distribution unlimited.		
17. DISTRIBUTION STATEMENT (of the abstract entered in Block 20, if different from Report)		
18. SUPPLEMENTARY NOTES		
19 KEY WORDS (Continue on reverse side if necessary and identify by block number)		

20 ABSTRACT (Continue on reverse side if necessary and identify by block number)

This report presents the results of an investigation in the design of a broadband quadruple-ridged waveguide radiator. It covers the theoretical and practical aspects in the design of the ridged waveguide parameters, the design of the ridges in the flared section, and the design of the coaxial to ridged waveguide transformer.

The result of the investigation is a 2 - 12 GHz bandwidth, dual-polarization, quadruple-ridged horn which is an advancement in the state-of-the-art.

DD FORM 1 JAN 73 1473 EDITION OF 1 NOV 65 IS OBSOLETE

UNCLASSIFIED

SECURITY CLASSIFICATION OF THIS PAGE (When Data Entered)

DISPOSITION INSTRUCTIONS

DESTROY THIS REPORT WHEN IT IS NO LONGER NEEDED. DO NOT RETURN IT TO THE ORIGINATOR.

DISCLAIMER

THE FINDINGS IN THIS REPORT ARE NOT TO BE CONSTRUED AS AN OFFICIAL DEPARTMENT OF THE ARMY POSITION UNLESS SO DESIGNATED BY OTHER AUTHORIZED DOCUMENTS.

TRADE NAMES

USE OF TRADE NAMES OR MANUFACTURERS IN THIS REPORT DOES NOT CONSTITUTE AN OFFICIAL INDORSEMENT OR APPROVAL OF THE USE OF SUCH COMMERCIAL HARDWARE OR SOFTWARE.

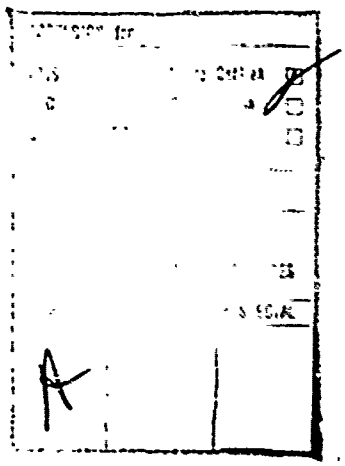

CONTENTS

ACKNOWLEDGEMENTS

My thanks are expressed to Mr. William L. Low, Chief, Radar Technology Branch, Advanced Sensors Directorate, and Mr. William J. Lindberg, Director, Advanced Sensors Directorate, US Army Missile Research. Development and Engineering Laboratory, US Army Missile Command, for their encouragement and cooperation in this work.

I also wish to acknowledge that without the full cooperation of personnel of the Boeing Aerospace Company, Research and Engineering Division, Seattle, Washington, this report could not have been written.

Section I. INTRODUCTION

This report presents the results of an investigation in the design of a broadband quadruple-ridged waveguide radiator. Since a quad-ridged horn element is used in the US Army Radio Frequency Simulation System (RFSS) target array, the design was undertaken to reduce the development risk in achieving a horn which would meet the RFSS antenna requirement.

The electrical performance characteristics for the horn are shown in Table 1. These characteristics are to meet the test conditions and limits so specified in Table 2. The desired antenna requires high spatial volume efficiency over a wide frequency range. Consideration of broadband antennas naturally leads to consideration of psuedo-infinite log-periodic antennas which have proven useful on so many applications. Log-periodic antennas, however, are limited to a gain of approximately 10 dB independent of the frequency. This means that while the antenna may have a very high volume efficiency at the low frequencies, the efficiency at the higher frequencies may not be all that is desired.

Horn antennas have high aperture efficiencies but have been capable of operating over only limited bandwidths. To extend the limited bandwidths, ridges have been added in recent years to the waveguide and flared sections of the horns. Since the design requires an antenna capable of producing circular polarization with two ports, a square geometry would be necessary. Another important design parameter was the cross-polarization coupling on beam axis between the two ports. It was this parameter that eliminated all consideration of log-periodic antennas, since tests of suitable antennas revealed results on the order of -12 dB rather than the -20 dB design specification. Narrow band quad-ridged horns had been tested and had cross-polarization couplings of the desired magnitude.

TABLE 1. ELECTRICAL PERFORMANCE CHARACTERISTICS

Parameter	Limit		Units
	Minimum	Maximum	
Frequency range (continuous)	2.0	12	GHz
Number of ports	2	2	
Gain on beam axis (at each port)	6.0		dBI
Pattern characteristics			
Symmetrical beam with maximum on axis			
Front-to-back lobe ratio	10		dB
Cross-polarization coupling on beam axis		-20	dB
Port isolation	25		dB
Amplitude imbalance between ports		0.5	dB
Phase imbalance between ports		10	degrees
VSWR at each port		2.0:1	
Port connectors (2)			female type SMA
Gain spread among antennas (at any frequency within band)		1	dB
Power handling capability			
Peak power	10	100	Watt
duty factor (average power) 25%	2.5	25	Watt

TABLE 2. ELECTRICAL TEST METHODS AND PARAMETER VALUE LIMITS

Parameter	Suggested Method or Other Mutually Agreed Method	Limit		Units
		Minimum	Maximum	
Frequency Range	Standard frequency measurement method	2.0	12.0	GHz
Gain/Pattern	Measure received signal level versus angular coordinates in E&H principal E&H radiation planes of test horn at each port with the other port terminated in a 50 ohm load at 2, 5.5, 10, 12 GHz. Do the same with a linearly polarized standard-gain horn and compare signal levels of test horn with that of the standard-gain horn.	6 (on axis) Symmetrical beam on axis 10 dB (front to back ratio)		dBi
Cross-Polarization Coupling	Measure with a swept frequency system; with test horn on receive and aligned on beam axis relative to a linearly polarized incident wave, measure and record signal levels between two orthogonal ports; do the same with orthogonal linear polarization.		-20	dB
Port Isolation	Measure with a swept frequency system; with test horn on transmit, measure and record signal levels between orthogonal ports; do the same for each port.	25		dB
Amplitude Imbalance	Measure with a swept frequency system; compare signal level of the test horn relative to that of a reference antenna for each linear polarization; reference antenna to be defined.		0.5	dB

TABLE 2. CONCLUDED.

Parameter	Suggested Method or Other Mutually Agreed Method	Limit		Units
		Minimum	Maximum	
Phase Imbalance	Same as amplitude imbalance measurement except the phase of the signal of the test horn relative to that of a reference antenna is compared for each linear polarization.		10	deg
VSWR	Measure with a swept frequency system at each port with the other port terminated in a 50 ohm load.		2.0:1	
Gain Spread	Compare gain measurements from antenna to antenna at each port.		1	dB
Power Handling Capability	Use a power source capable of delivering the specified power level and duty factor at X-band. Feed this power into test horn; gradually increase the power level and record the transmit power with a linearly polarized receiving horn on beam axis. At each power level, compare received power level at two orthogonal orientation of the linearly polarized horn.	10 peak 2.5 Avg	100 peak 25 Avg	W W
Random Drop	Per MIL-STD-202, Method 203A, measure port isolation and VSWR before and after test. All parameters shall meet the limits as specified above.			
Vibration	Per MIL-STD-202, Method 204, test condition C, rigid mounting, resonance search equipment used to determine resonance points. Measure port isolation and VSWR before and after test. All parameters shall meet the limits as specified above.			

Section II. STATEMENT OF THE DESIGN PROBLEM

It is the goal of this paper to dwell on the theoretical and practical aspects of designing a quadruple-ridged waveguide radiator rather than on the aspects of pyramidal horn design. The exterior dimensions of the horn were selected consistent with the dimensions of the feeding waveguide, the 6 dBI minimum gain requirement at the lower end of the frequency band, and minimization of phase errors across the aperture. This later constraint is especially true when extremely wide bandwidths are considered. Since the ridges must be terminated within the flared section, the horn aperture must be half a wavelength or more in width (H-plane) at the lowest frequency to permit propagation of the TE_{10} mode.

However, an aperture more than a half wavelength wide at the lowest frequency is many wavelengths wide at the highest frequency. This means that large phase errors will be present across the aperture unless the horn is extremely long. This can be a limiting factor at the high end of the frequency band of operation of ridged horns. Sometimes a dielectric lens is used to reduce the phase error to a minimum.

Figure 1 shows the broadband quadruple-ridged waveguide radiator. It looks like an ordinary pyramidal horn. An open view is depicted in Figure 2, and Figure 3 gives an open view on a coax feed-side of the horn. The basic horn configuration, as seen from the three figures, consists of quadruple-ridged waveguide terminated at one end in a waveguide to coax transformer and at the other end in the flared horn section. Selection of the ridged waveguide parameters will be discussed in Section III. Design of the ridges in the flared section is covered in Section IV and the coaxial to ridged waveguide transformer design is in Section V.

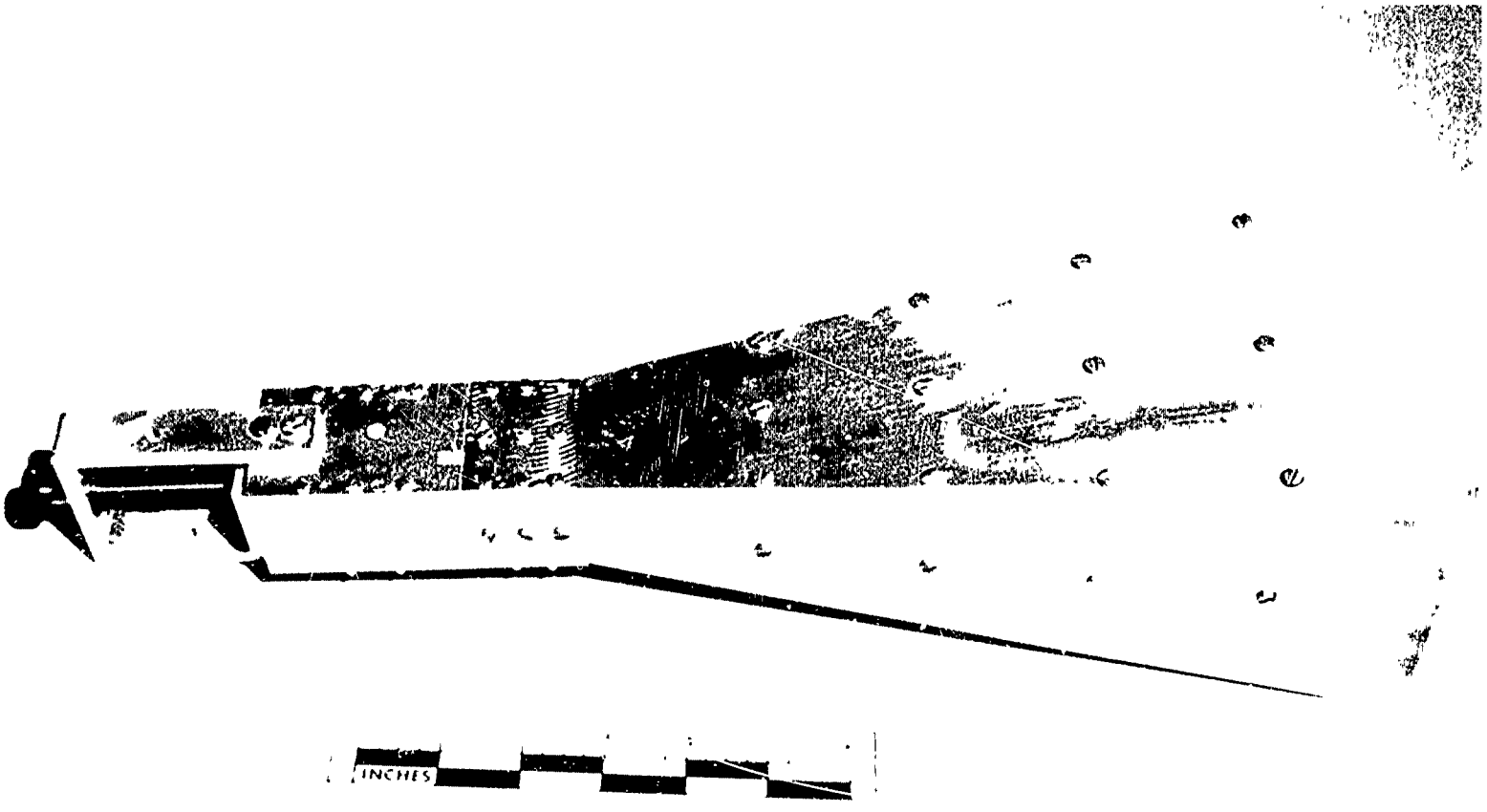

Figure 1. Broadband quadruple-ridged waveguide radiator.

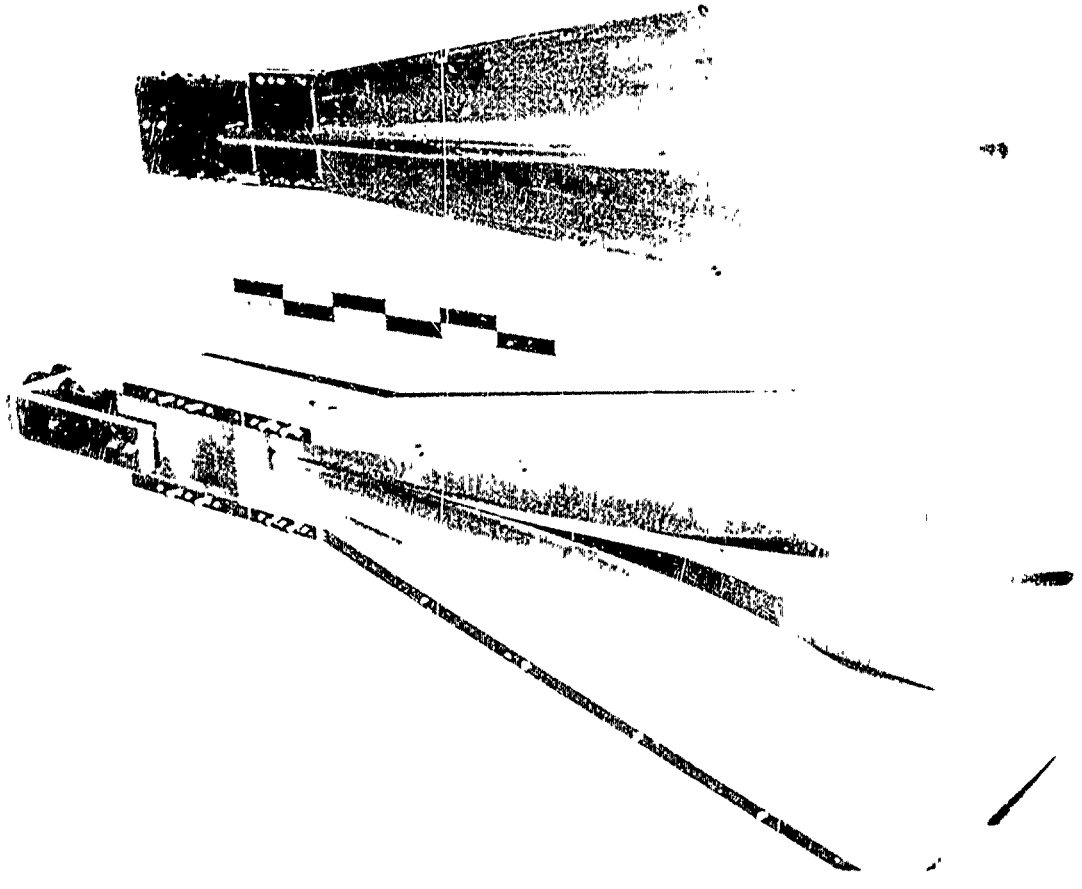

Figure 2. Open view of waveguide radiator.

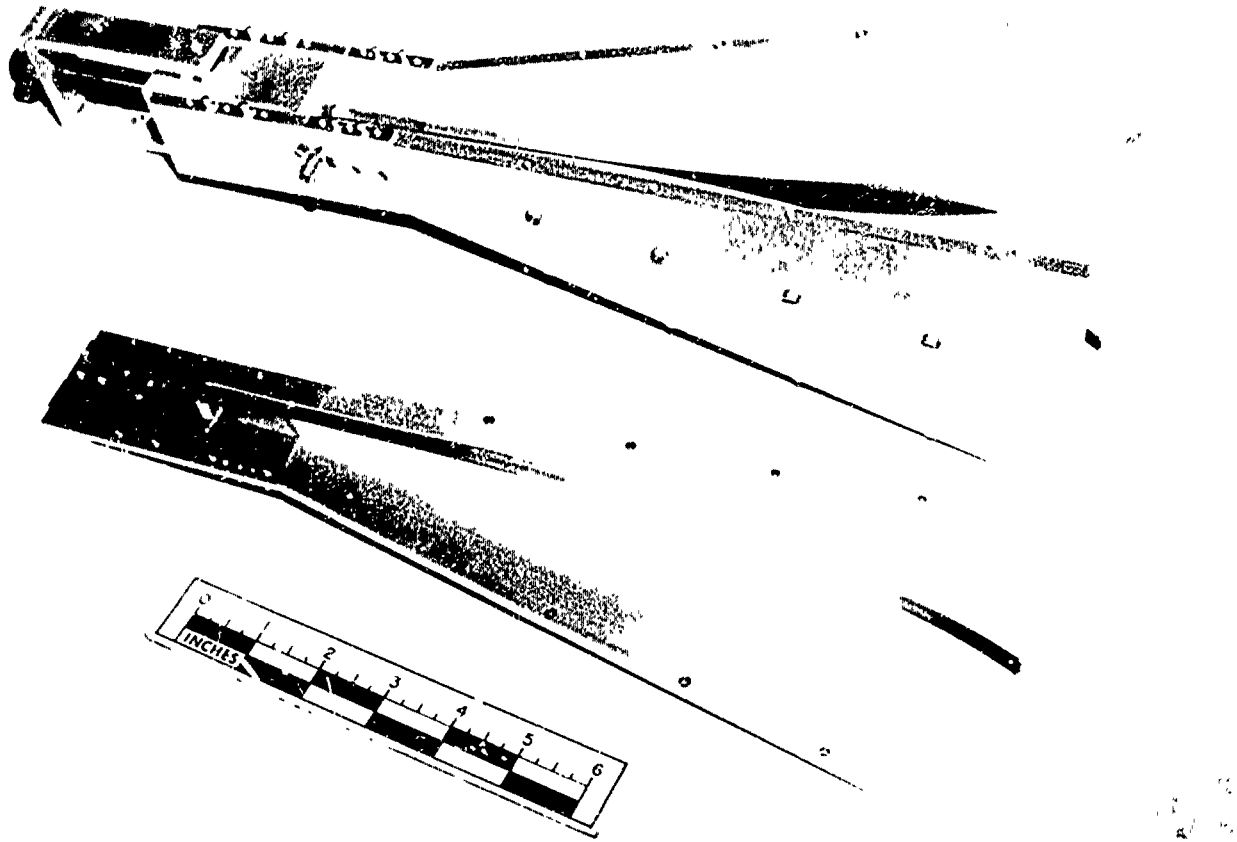

Figure 3. Feed-side view of waveguide radiator.

Section III. RIDGED WAVEGUIDE PARAMETERS

Ridged waveguides have been useful for several years in microwave systems requiring broadband operation. Much theoretical and practical work has been done. In 1947 Cohn [1] published waveguide eigenvalues obtained by using transverse resonance to formulate transcendental equations. The discontinuity susceptance between parallel plate waveguides obtained by Whinnery and Jamieson [2] was employed in the calculations. In 1955 Hopfer [3] extended Cohn's work to other aspect ratios by inclusion of a first-order correction factor. Hopfer used a quasi-static solution for the discontinuity susceptance between parallel plates obtained from Marcuvitz [4]. In 1964 Walton and Sundberg [5] extended the analysis to cover a broad range of aspect ratio's and applied these results to the design of broadband, linearly polarized horns. Hopfer's work was further extended in 1966 by Pyle [6] to accurate data for any aspect ratio. Additionally, Pyle included an analysis of error effects.

Each of these previous investigations was primarily aimed at the solution for the TEno eigenvalues. Little was said about the fields of ridged guide until 1961 when Getsinger [7] formulated approximate field equations by assuming a TEM mode at the gap and matching only the electric field. Getsinger used the eigenvalues obtained by Hopfer. A more complete analysis was presented by Montgomery [8] in 1971. The solution is obtained by the formulation of an integral eigenvalue equation which is subsequently solved numerically by application of the Ritz-Galerkin method.

All of the previously mentioned papers concern themselves with the single or double-ridged waveguide problem. Sexson [9] in 1966 did some analysis on the quadruply-ridged horn. A perturbation technique is used to determine the TEno cutoff frequencies when the ridges are small, and a transverse resonance technique is used when the ridges are large. More recently, with the increased interest in wideband, circularly polarized radiators in phased array antennas, additional work has been done in 1973. C. C. Chen [10] et al. designed some radiators with four ridges, while M. H. Chen and Tsandoulas [11,12] determined the modal characteristics of quadruple-ridged circular and square waveguide. Their analytical study is based on a computer program that calculates the eigenvalues and scalar potentials for an arbitrarily-shaped waveguide. The analysis was developed by Konrad and Sylvester [13] using the triangular-finite-element method.

In the actual design of the ridged waveguide parameters, it was assumed that a simpler two-ridge analysis could be carried directly to the four-ridge geometry. Once the actual geometry was settled upon based on a parametric study of the simpler equations and curves for a two-ridge geometry, a final verification for the four-ridge geometry was obtained by the computer work of Chen and Tsandoulas.

The geometry selected is shown in Figure 4, with the letter notation that used by Chen and Tsandoulas. Figure 5 shows Cohn's [1] single-ridged geometry with the shaded portion indicating that use of his equations would be an approximation to the pointed ridges. This is true also for Walton and Sundberg's [5] geometry shown in Figure 6. They consider flat ridges only. Locating the feed probe in the center of the waveguide and using a short straight section of ridged waveguide, as the wave launcher, precludes exciting the TE_{20} mode so that the maximum usable bandwidth is the ratio of TE_{10} to TE_{30} mode cutoff wavelengths $(\lambda_c^{10}/\lambda_c^{30})$ rather than $(\lambda_c^{10}/\lambda_c^{20})$.

The simpler equations for the cutoff wavelengths of the various modes are as follows:

$$\frac{B}{D} \tan \theta_2 - \cot \theta_1 + \frac{B_C}{Y_{01}} = 0 \qquad (1)$$

$$\frac{B}{D} \cot \theta_2 + \cot \theta_1 - \frac{B_C}{Y_{01}} = 0 \qquad (2)$$

where all notation is that for Figure 6 and

$$\theta_1 = \frac{360}{\lambda_C} \left(\frac{A - S}{2}\right) \text{ degrees}$$

$$\theta_2 = \frac{360}{\lambda_C} \left(\frac{S}{2}\right) \text{ degrees.}$$

The value of the discontinuity susceptance term (B_C/Y_{10}) is derived by Whinnery and Jamieson [2], and Equation (1) applies to TE_{M0} modes where M is odd while Equation (2) applies where M is even.

Hopfer [3] has derived an expression for the characteristic impedance of ridged waveguides for the TE_{10} mode at infinite frequency which is as follows:

$$Z_{0\infty} = \frac{1}{Y_{0\infty}}$$

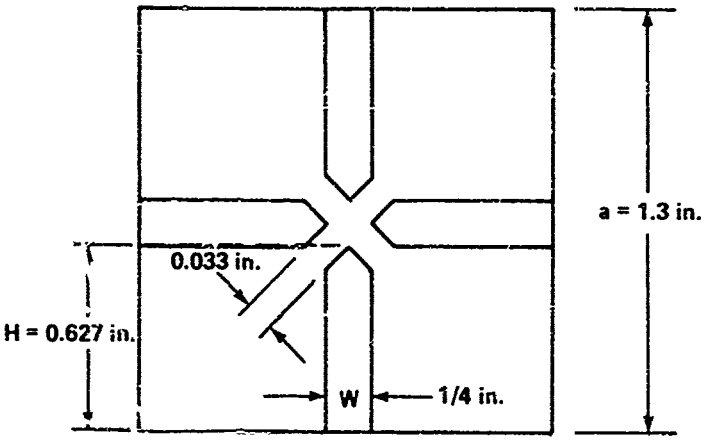

Figure 4. Ridged waveguide parameters.

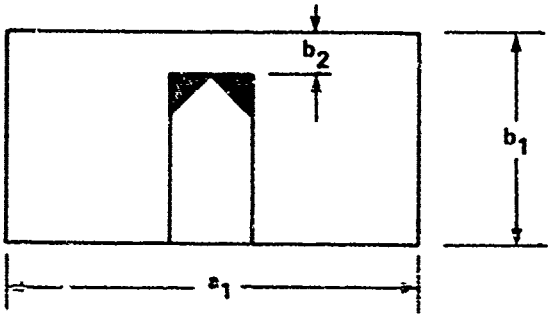

Figure 5. Cohn's waveguide parameters.

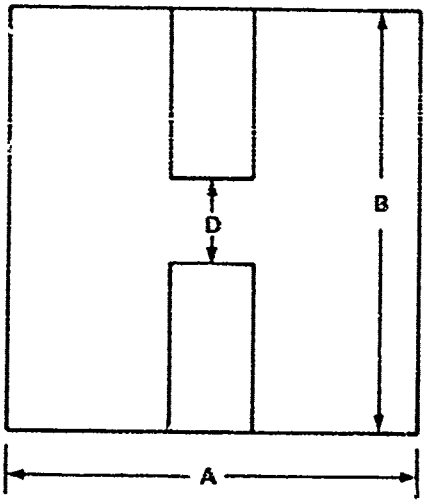

Figure 6. Walton and Sundberg's waveguide parameters.

where

$$Y_{0\infty} = 2\sqrt{\frac{\epsilon_0}{\mu_0}}\ \frac{\lambda_c}{2\pi D}\left\{\frac{2D}{\lambda_c}\cos^2\left(\frac{\pi S}{\lambda_c}\right)\ \ell n\ \csc\left(\frac{\pi D}{2B}\right)\right.$$

$$+\frac{\pi S}{2\lambda_c}+\frac{1}{4}\sin\left(\frac{2\pi S}{\lambda_c}\right)+\frac{B}{D}\ \frac{\cos^2\left(\frac{\pi S}{\lambda_c}\right)}{\sin^2\left(\frac{\pi}{\lambda_c}(A-S)\right)}\left[\frac{\pi(A-S)}{2\lambda_c}\right.$$

$$\left.\left.-\frac{1}{4}\sin\left(\frac{2\pi(A-S)}{\lambda_c}\right)\right]\right\} \qquad (3)$$

The characteristic impedance at a frequency F is given by

$$Z_0 = \frac{Z_{0\infty}}{\sqrt{1-\left(\frac{F_c}{F}\right)^2}} \quad . \qquad (4)$$

Previously published curves of λ_c^{10} and λ_c^{30} may prove to be adequate to provide the necessary range of waveguide parameters. If not, then additional calculations will need to be performed. Figure 7 presents a set of curves from Cohn's paper with the notation used as seen in Figure 5. Using actual values derived from Figure 4, the waveguide parameter ratios become:

$$\frac{b_2}{b_1} = 0.035,\ \frac{a_2}{a_1} = 0.1923,\ \frac{b_1}{a_1} = 0.5 \quad .$$

Noting that $\lambda_c = 2a_1$, these ratios give the TE_{10} cutoff frequency at approximately 1.2 GHz. Cohn's curves also give $Z_{0\infty}$ at approximately 68 ohms. An actual calculation of $Z_{0\infty}$ for a cutoff frequency of 1.2 GHz using Cohn's impedance formula gives $Z_{0\infty} = 63.5$ ohms for double-ridged waveguide. Cohn also calculated the cutoff ratios for the TE_{30} modes as shown in Figure 8. Using previously calculated waveguide parameter ratios, the TE_{30} cutoff frequency lies between 11.2 GHz and 11.3 GHz.

Walton and Sundberg calculated the curves shown in Figure 9. The B/A = 0.9 is fairly close to the actual B/A = 1.0 ratio. The other ratios are S/A = 0.1923 and D/B = 0.0354. Therefore one can obtain from Figure 9 the TE_{10} cutoff at approximately 1.2 GHz, the TE_{30} cutoff at approximately 11.5 GHz, and $Z_{0\infty}$ at approximately 40 ohms. An actual

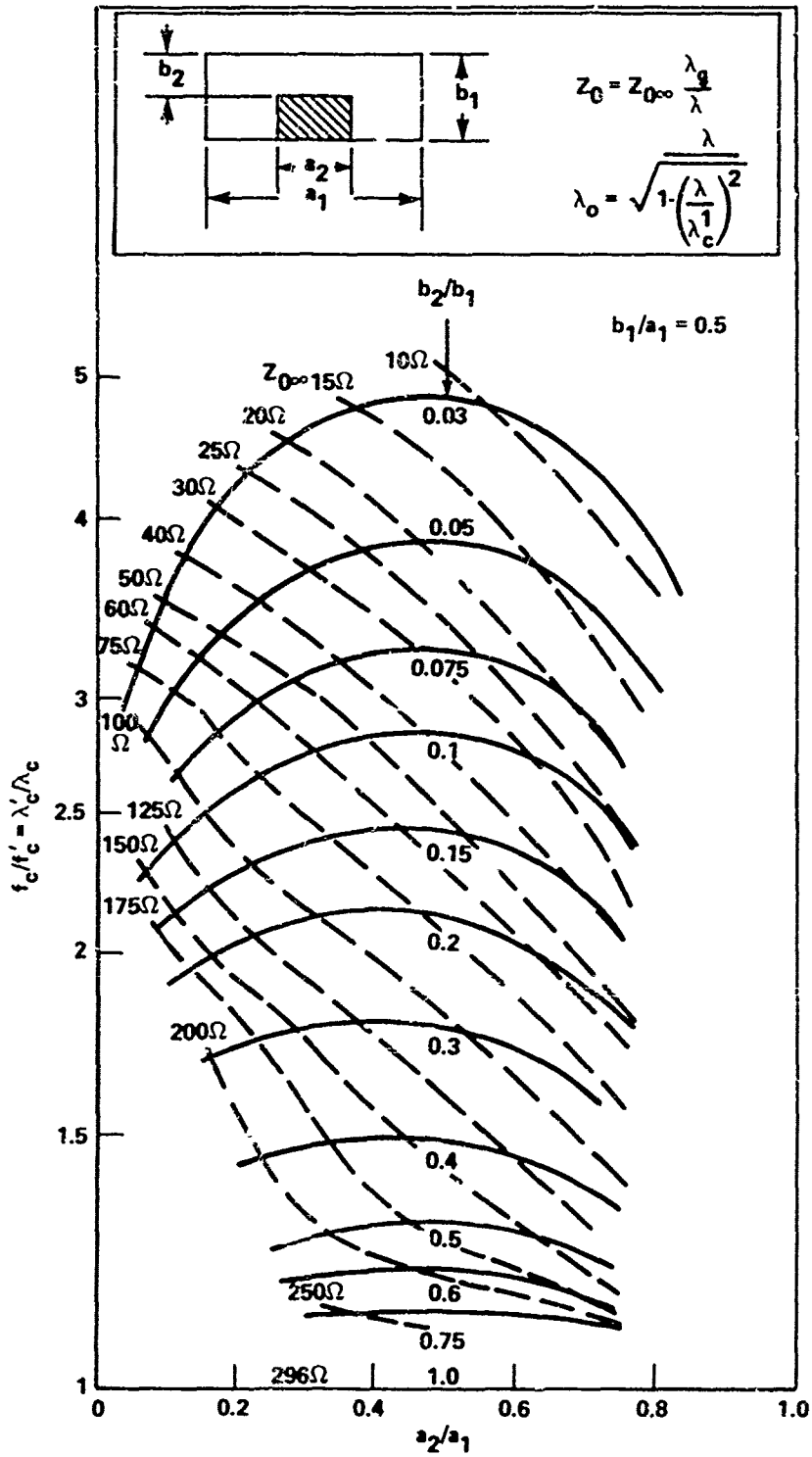

Figure 7. Characteristic impedance and cutoff wavelength of ridge waveguide ($b_1/a_1 = 0.5$).

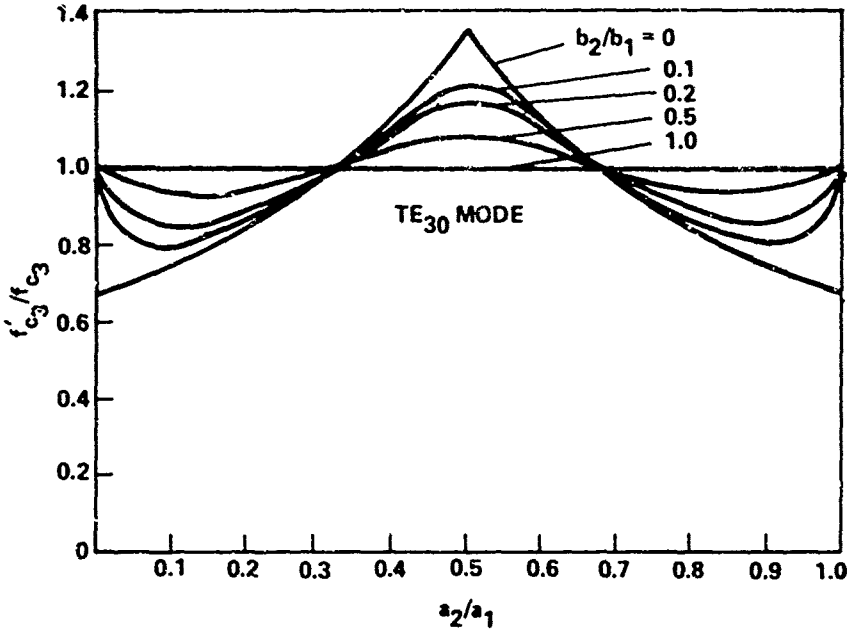

Figure 8. Cutoff-frequency ratios for the TE_{30} modes in ridge waveguide.

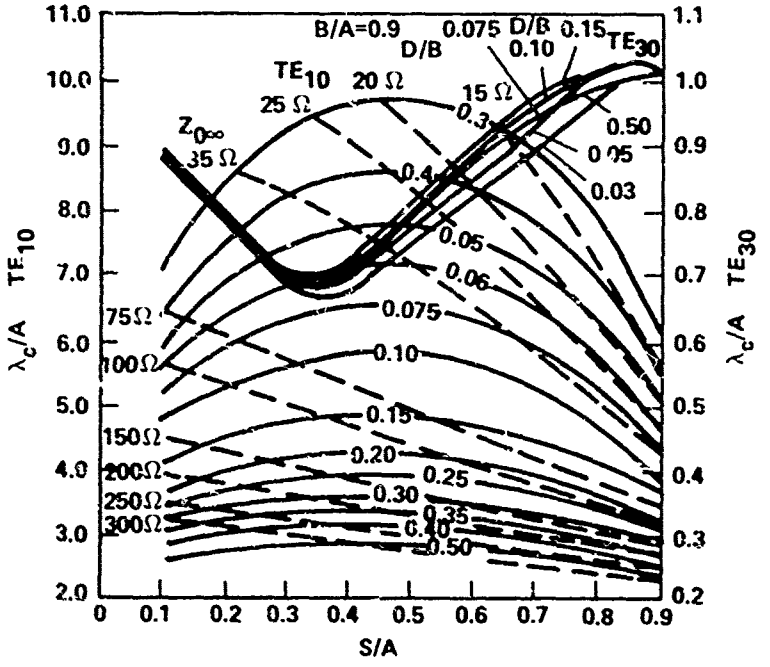

Figure 9. TE_{10} and TE_{30} mode cutoff wavelengths in doubly-ridged waveguide. $Z_{0\infty}$ is also shown. B/A = 0.9.

calculation of $Z_{0\infty}$ using Hopfer's more accurate impedance equation, Equation (4), and TE_{10} cutoff at 1.2 GHz gives $Z_{0\infty}$ = 50.11 ohms.

These results indicate that the geometry selected for the quadruply-ridged waveguide seems fairly sufficient in bandwidth and impedance. Some concern was given to the possibility of TE_{30} modes at approximately 11.5 GHz but it was hoped that these modes would not be excited. As a verification of the approximations made in going from two flat-ridged waveguide to the pointed-ridged waveguide, correspondence was made with H. H. Chen for use of his computer program. His program solves the scalar, two-dimensional Helmholtz equation,

$$(\nabla^2 + k_c^2)\ \Phi(x,y) = 0 \qquad (5)$$

subject to proper boundary conditions. Since the scalar potential represents either the longitudinal magnetic field, H_z, for the TE modes or the longitudinal electric field, E_z, for the TM modes, the boundary conditions for these modes are respectively $\partial\Phi/\partial n = 0$ and $\Phi = 0$. The solutions of Equation (5) are eigenvalues, k_{c_i}, and eigenfunctions, $\Phi_i(x,y)$. The k_{c_i} may be related to the modal cutoff frequency and the $\Phi_i(x,y)$ may be related to the field distribution for mode i in the waveguide.

The actual geometry as shown in Figure 4 was utilized in the calculations by Chen and Tsandoulas. Results are shown in Figure 10 for W/a = 0.1923. The actual H = 0.627 inch, a = 1.3 inches gives a ratio H/a of about 0.48 and reading from Figure 10 gives the TE_{10} cutoff frequency at 1.36 GHz and 11.36 GHz as the cutoff frequency for TE_{30} mode. Thus the assumption of utilizing double-ridge analysis for quadruple-ridge geometry seems to be a good one. Figure 10 also shows that the geometry selected can support several other propagating modes at frequencies lower than the TE_{30} mode cutoff frequency of 11.36 GHz. These modes will not be excited with the selection of the feed at the center of the ridges.

Figure 11 shows the bandwidth (TE_{10} - TE_{30}) versus H/a characteristics for the W/a = 0.1923 ratio. The bandwidth is computed from the relation,

$$BW = \frac{\lambda_{10} - \lambda_{30}}{\lambda_{10} + \lambda_{30}} \times 200\% \qquad (6)$$

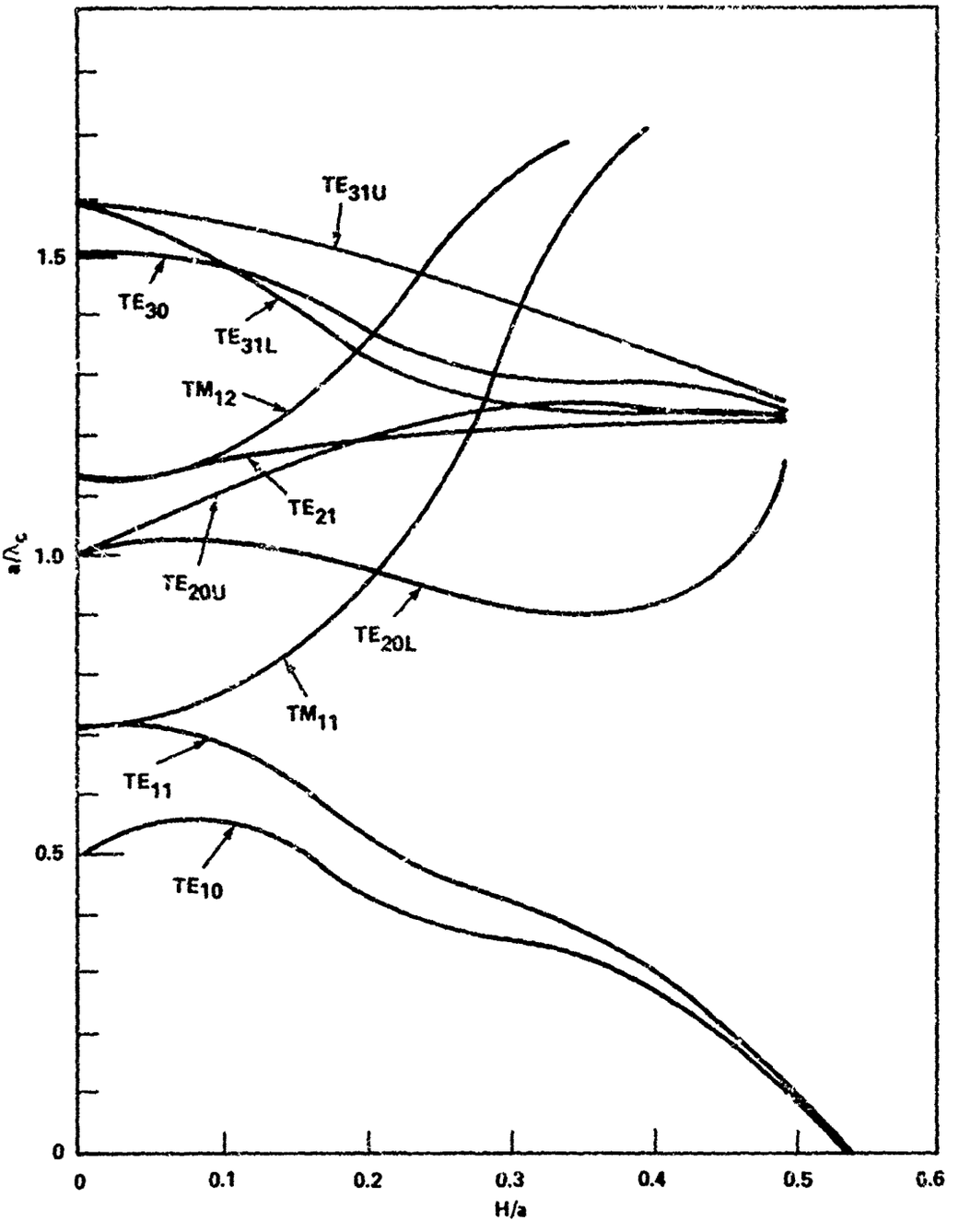

Figure 10. Modal cutoffs versus H/a characteristics for quadruple-ridged square waveguide.

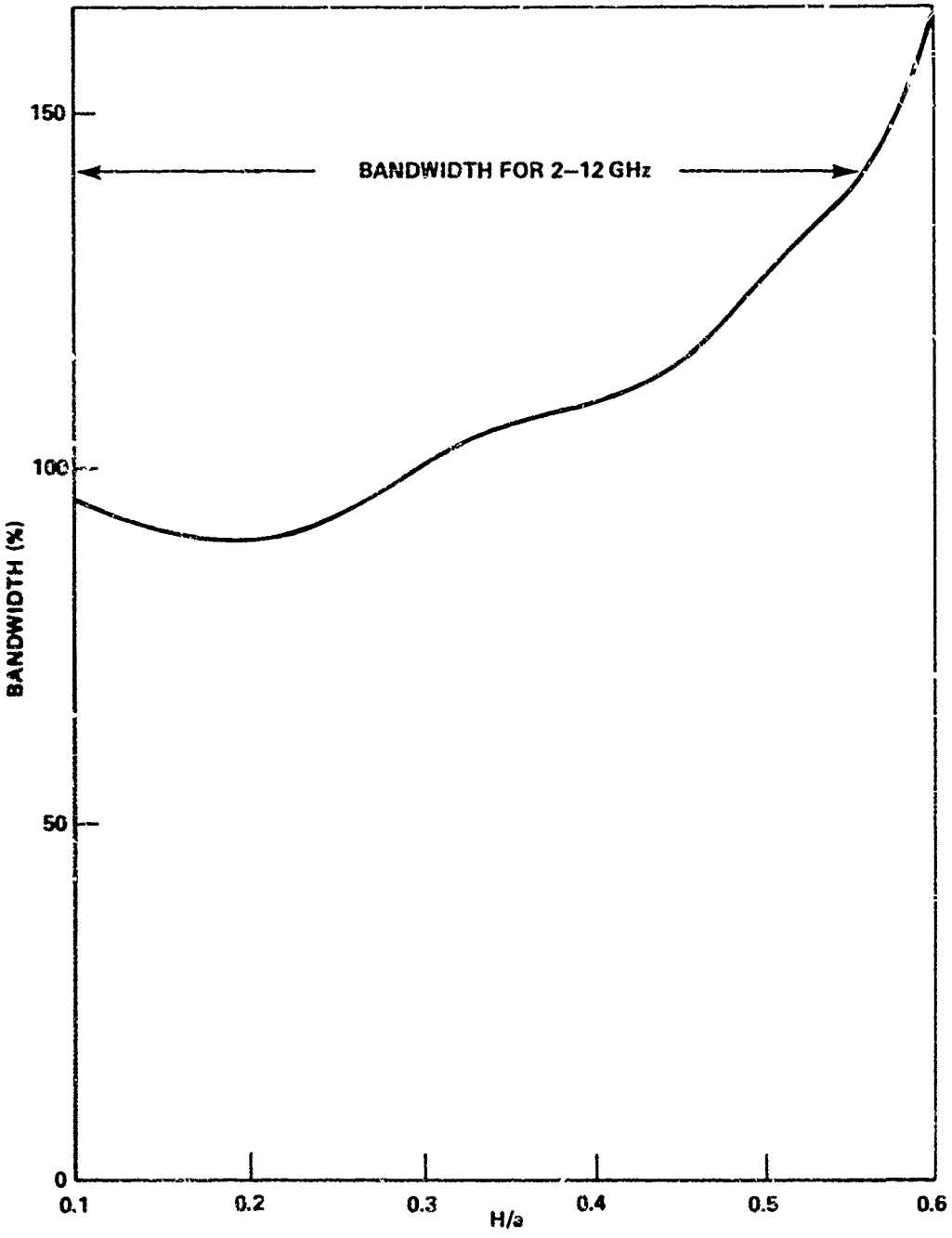

Figure 11. Bandwidth (TE_{10} - TE_{30}) versus H/a characteristics for quadruple-ridged square waveguide.

where λ_{10} and λ_{30} are the TE_{10} and TE_{30} cutoff wavelengths, respectively. The value of BW thus obtained is as a percentage of the center frequency between the two modal cutoffs.

The transverse field distribution for quadruple-ridged square and circular waveguides can be obtained from the computed scalar potential $\Phi(x,y)$. The scalar potential represents the longitudinal component of the magnetic field for TE modes and of the electric field for TM modes. Therefore, the transverse electric and magnetic fields can be derived from

$$\left.\begin{aligned} \underline{H}_t(x,y) &\sim \nabla_t \, \Phi_{TE}(x,y) \\ \underline{E}_t(x,y) &\sim \underline{Z}_0 \times \nabla_t \, \Phi_{TE}(x,y) \end{aligned}\right\} \quad \text{TE modes}$$

$$\left.\begin{aligned} \underline{E}_t(x,y) &\sim \nabla_t \, \Phi_{TM}(x,y) \\ \underline{H}_t(x,y) &\sim \underline{Z}_0 \times \nabla_t \, \Phi_{TM}(x,y) \end{aligned}\right\} \quad \text{TM modes} \; . \qquad (7)$$

Accordingly, the equipotential lines represent electric field lines for the TE modes and magnetic field lines for the TM modes.

Figures 12 and 13 show the electric field patterns for the TE_{10} and the TE_{30} modes, respectively. The figures represent one-fourth of the actual geometry. The other three-fourths is symmetric with the portion shown. The field patterns for the dominant TE_{10} mode indicate that most of the electric field is maintained within the ridges as seen in Figure 12. For the TE_{30} mode field patterns there are two maximums with a change in sign. This is one way to represent the TE_{30} moding, and indicate that there is more field intensity outside of the ridge gaps than for the TE_{10} mode case.

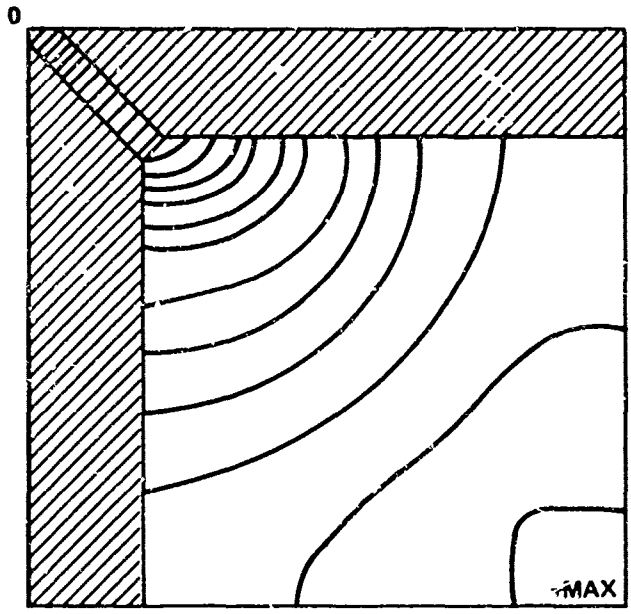

Figure 12. Electric field lines for TE_{10} mode.

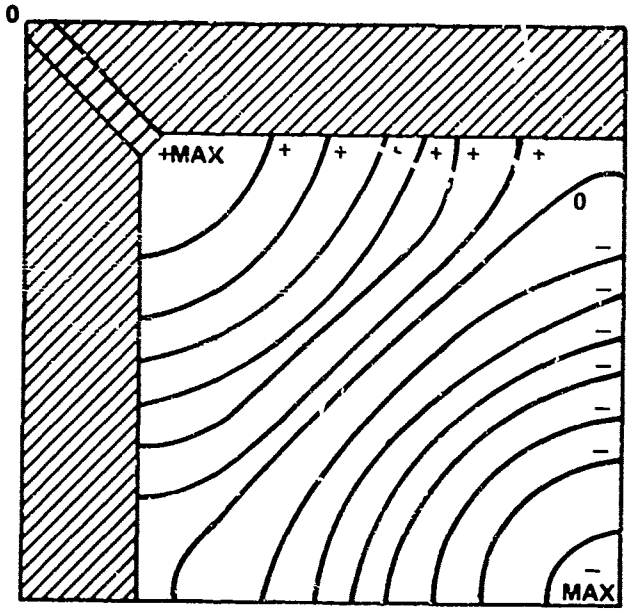

Figure 13. Electric field lines for TE_{30} mode.

Section IV. DESIGN OF THE RIDGES IN THE FLARED SECTION

In the design of the ridges in the flared section one notes that the ridges must be extended into the flared horn section past the point where the flared section becomes sufficiently wide to support the TE_{10} mode at the lowest operating frequency. It is desired that the ridge height and width taper must also be such that the associated impedance taper is a smooth transition from the ridge impedance of 50 ohms or less to the impedance of free space, 377 ohms.

Walton and Sundberg [5] found that an exponential impedance taper of the form

$$Z = Z_{0\infty}\, e^{kx} \quad ; \quad 0 \le x \le \frac{\ell}{2} \tag{8}$$

$$Z = 377 + Z_{0\infty}\left(1 - e^{k(\ell - x)}\right) \quad ; \quad \frac{\ell}{2} \le x \le \ell \tag{9}$$

is quite satisfactory. Here $Z_{0\infty}$ is the characteristic impedance of the waveguide and K is a constant such that the impedance of the midpoint of the flared section is the average of the end point impedances.

Kerr [14,15,16] superimposes an additional linear taper on a logarithmic curve. The amount of this additional linear taper has been determined experimentally in the design of double-ridged horns. They have ranged from 0.008 X inch to 0.020 X inch where the X-coordinates are axial distances measured along the center line of the antenna, beginning at the aperture plane of the launcher. He uses the Y-coordinates as perpendicular distances from the center line of the antenna to the radiating element surface.

The taper used in the actual horn design is shown in Figure 14. Constants of the horn taper design were calculated to be derived from the following formula for a 4.50 inch square aperture horn:

$$Y = 10^{0.192543\ X\ -\ 1.63827} + 0.020\ X \tag{10}$$

where the X and Y coordinates are depicted previously, and the 0.020 X additional linear taper is used. Kerr found that this additional linear taper serves to provide a significant improvement in the VSWR over the first octave of the bandwidth and has little effect elsewhere in the range of interest.

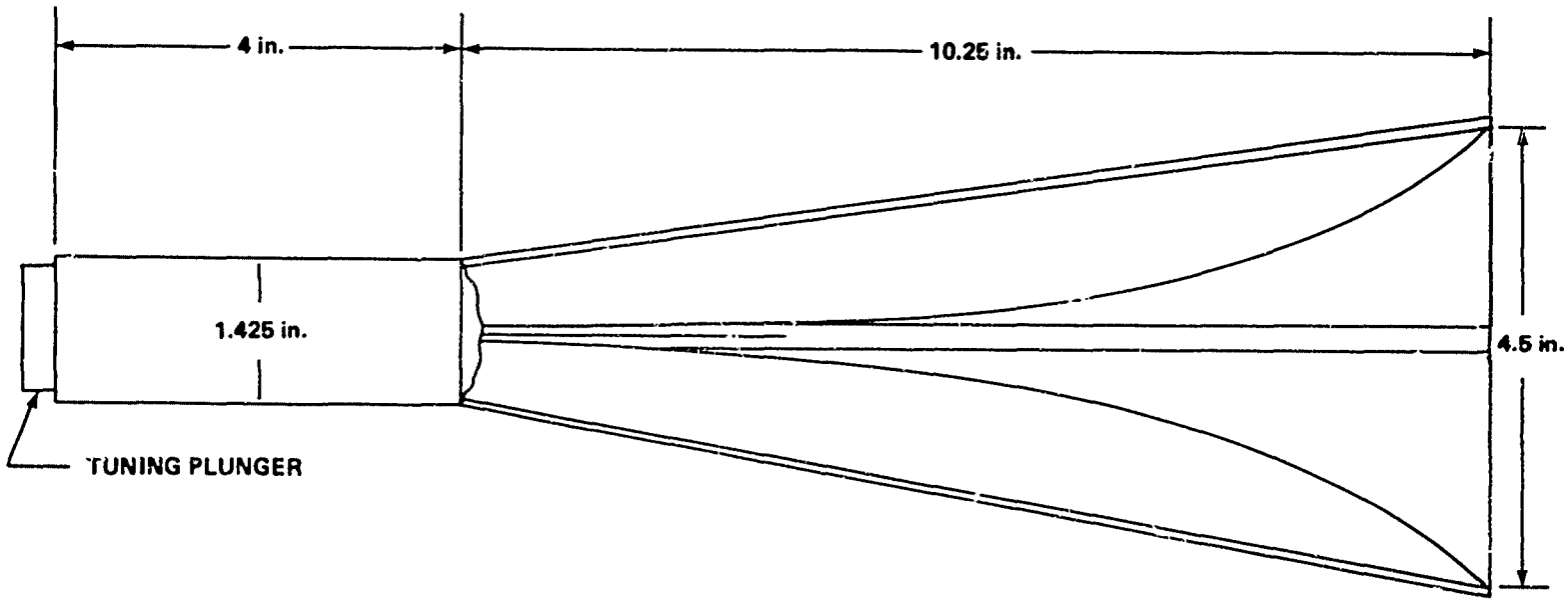

Figure 14. Quadruple-ridged waveguide radiator dimensions (side).

Section V. DESIGN OF THE COAXIAL TO RIDGED WAVEGUIDE TRANSFORMER

The previous sections have dealt with the design of the ridged waveguide and the design of the ridges in the flared section of the horn. This section will deal with the design of the coaxial to ridged waveguide transformer. The basic problem is to provide for a transition between the principal coaxial TEM mode and the dominant TE_{10} mode in the ridged waveguide. The fundamental way of establishing a desired mode in a waveguide is the excitation of either the electric or the magnetic field intensity with that mode. This is done either by means of an "antenna" element parallel to the electric field or by means of a loop, the plane of which is normal to the magnetic field. Although each type has had some application, transitions based on the waveguide "antenna" for electric coupling are much more widely used and is the method selected.

The crossed transition from coaxial line to waveguide is treated theoretically by Slater [17] who has shown that a transition of this type can be matched by variation of the end-plate and coaxial-plunger positions, dimensions D and S of Figure 15. In particular, the coaxial stub constitutes a variable reactance in series with the waveguide "antenna" (that portion of the coaxial center conductor which extends across the guide), and by means of variations in the length of the short-circuited section of guide, it is possible to adjust the radiation resistance of this "antenna." It has been found, however, by Ragan [18], Cohn [19], Walton and Sundberg [5], and Kerr [14-16] that an experimental approach to the design seems more expedient.

The approach taken in the design of the quadruple-ridged waveguide radiator was to construct two identical horns as shown previously in Figures 1, 2, and 3. These two horns had a movable piston in the back or short-circuited section of the guide. This allowed a movable D dimension. Once the horns were constructed, the design of the coaxial to ridged waveguide transformer was accomplished experimentally. Work was performed at Boeing, Seattle, and Redstone Arsenal, Alabama, simultaneously.

The final horn dimensions are shown in Figures 14, 16, and 17. Figures 14 and 16 show the side and front dimensions of the radiator, while Figure 17 shows the coaxial to ridged waveguide transformer. The coaxial connector is an OSM 206-2 flange mount connector for 0.085-inch semi-rigid cable. The center conductor or "antenna" of the coaxial cable is 0.020 inch in diameter.

Initially, the ridges did not have the angle θ cut into them. The two "steps" shown in Figure 17 also were not initially constructed. Measurements were made utilizing only the "piston" movement as a variable. Results indicated good characteristics up to approximately 8 GHz for an optimum setting of the "piston" or "plunger." The addition

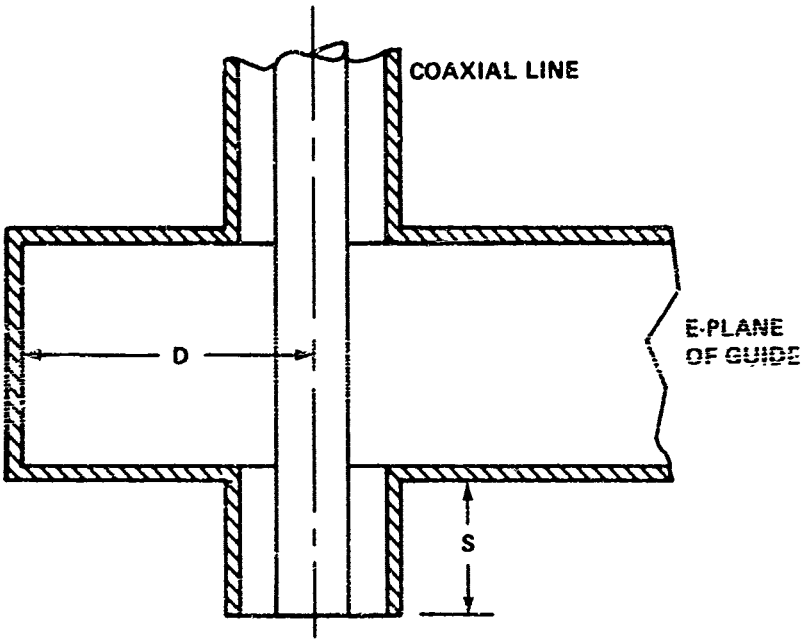

Figure 15. Slater's crossed transition for excitation of the electric field.

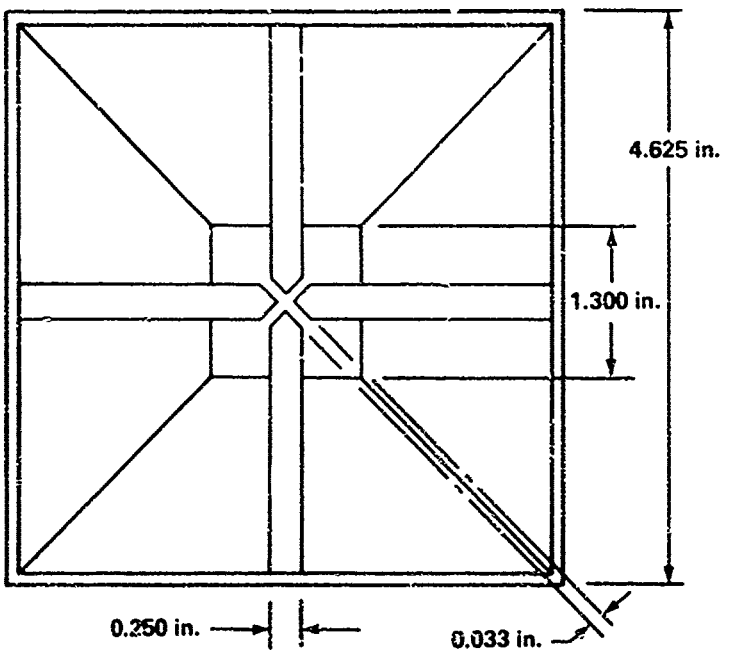

Figure 16. Quadruple-ridged waveguide radiator dimensions (front).

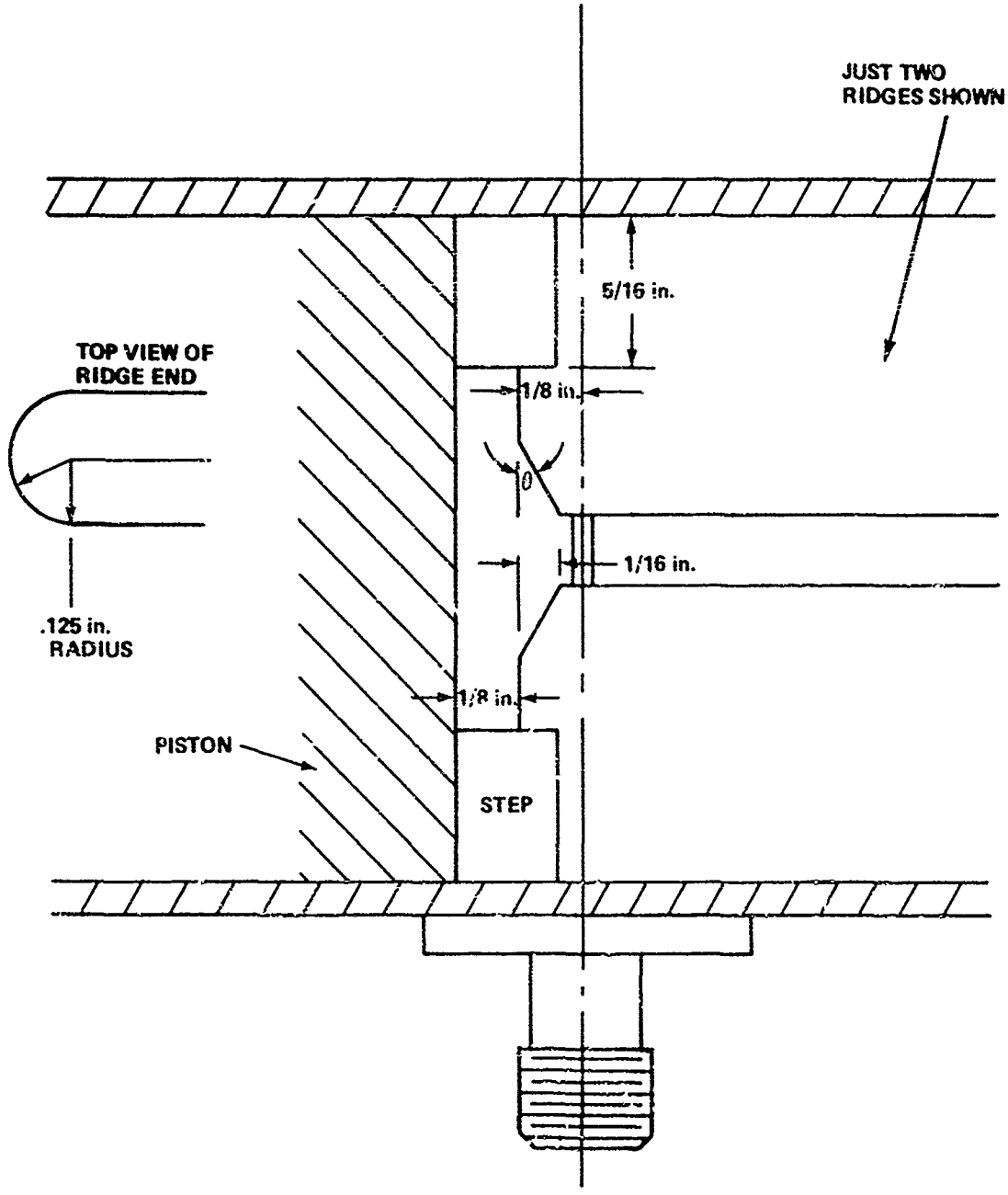

Figure 17. Coaxial to ridged waveguide transformer.

of the proper "steps" extended the antenna bandwidth up to approximately 10.5 GHz. Later the angle θ of approximately 30 degrees was cut into the ridges, and a metal sleeve was added to the antenna. The sleeve was 0.032 inch in diameter.

Only one pair of ridges is shown in Figure 17. Another pair exists with another feed orthogonal to the first antenna. Metal to metal separation is 0.020 inch or 0.030 inch. One antenna had the 0.020 inch separation and another the 0.030 inch separation. The only parameter that was noticeably affected by this difference in antenna separation was the phase imbalance between ports. The closer the separation, the better the phase imbalance between ports. This phase imbalance is not a critical consideration as one can offset the coaxial cable flange mount from the surface of the radiator to "make up" for the phase imbalance. A 0.020 inch offset for a 0.020 inch separation seems adequate to meet the design specification. Likewise for the 0.030 inch separation case, an offset of 0.030 inch is adequate.

Since the second feed or antenna is further away from the short-circuited part of the transformer, it was found that a deeper ridge cut was necessary than indicated for the first feed pair of ridges. The angle θ is approximately 42 degrees for the 0.030 inch separation antenna. These deeper cuts are necessary for fine tuning the design for the VSWR parameter in the specifications, but the actual dimensions are not critical in the precision machining sense. Only the gap separation between ridges require precision machining.

Care must also be taken in the construction of the coaxial feeds. As shown in Figure 17, the coaxial feed is inserted into a hole in the bottom ridge, and the center conductor (sleeve not shown) continues across the gap between the ridges into a hole in the top ridge. A set screw anchors the center conductor in the top ridge for good electrical contact. The hole in the bottom ridge may be drilled for either the dielectric portion of the coaxial cable or the outer conductor of the coaxial cable. Although both antenna horns constructed had holes drilled for the entire coaxial cables, it is recommended that holes be drilled for the smaller dielectric diameter. The reason for this is that the ridges are pointed. A dielectric entrance into the gaps between the ridges creates less of a perturbation than one with both metal outer conductor and dielectric. In the latter case, the outer conductor must not protrude into the gap regions. In both cases, the dielectric stops at the apex of the ridge point.

Section VI. EXPERIMENTAL RESULTS

The electrical performance characteristics for the broadband quadruple-ridged waveguide radiator are shown in Table 1. Actual experimental results of the horns designed are compared to these desired specification values.

Figure 18 shows the gain characteristics of the MICOM horn. The values used in the plot of Figure 18 are derived from a comparison of the measured patterns with that of a standard gain horn. Patterns of the E-plane and H-plane are taken at 2, 4, 5.5, 8, 10, and 12 GHz. In each pattern, the amplitude or gain on main beam axis of the standard gain horn is indicated by a marker. These patterns also give the amplitude imbalance between the two ports of the horn. The solid pattern is for one port (Port No. 1) while the dotted pattern is for the corresponding port (Port No. 2). The results indicate that the patterns are symmetrical with the maximum on the main axis. Gain is well above the specified values, while amplitude imbalance is near the 0.5 dB specification. These patterns are found in the appendix.

The appendix also contain plots of the on-axis-polarization patterns at 2, 4, 5.5, 8, 10, and 12 GHz. In Figure A-3 of the appendix, a cross-polarization of 18.5 dB is indicated. Actually, one should read the difference between a peak and a null of the same pattern, rather than a null from the pattern of one port and a peak from the pattern of the corresponding port. However, reading the cross-polarization as indicated in Figure A-3 is good enough as patterns are within one-half dB of each other. The value of 18.5 dB is the only value out of the specification value of 20 dB. It should be noted that the other port has a cross-polarization value of approximately 30 dB at 2 GHz.

It should be noted that swept frequency measurements of gain, amplitude-imbalance, and cross-polarization coupling were taken as specified in Table 2, but only a representative part of the data is shown in this report.

Figure 19 presents consolidation of the isolation characteristics of the MICOM horn, and Figure 20 shows the phase imbalance between ports. Figure 20 is shown only to indicate what the phase imbalance is without any coaxial-line adjustments in the feed probes. The two probes or antennas inside the gap of the ridges are 0.030 inch apart. As discussed earlier, an offset of the coaxial cable flange mount from the surface of the radiator can "make up" for the phase imbalance shown in Figure 20. Values of approximately 5 degrees were achieved.

The VSWR characteristics of the MICOM horn with two gap widths are shown in Figures 21 and 22. All data previously indicated were for the MICOM horn with the 0.030 inch probe separation and 0.033 gap width. By reducing the gap width to 0.026 inch, one improves the VSWR without changing the other characteristics very much. This lowers the peak VSWR points from 2.5:1 to 2.3:1 in the 2 - 12 GHz frequency band.

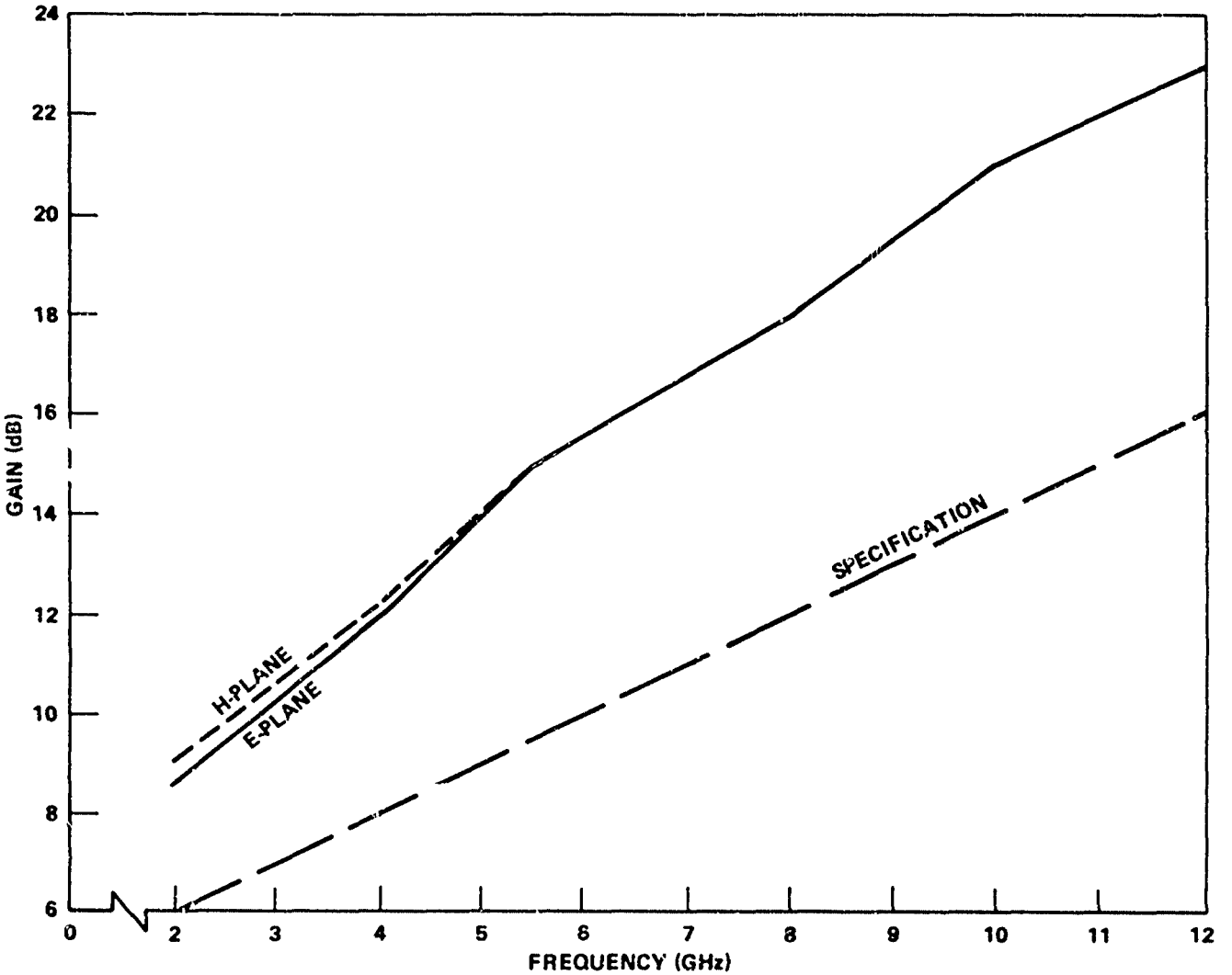

Figure 18. Gain characteristics of MICOM horn.

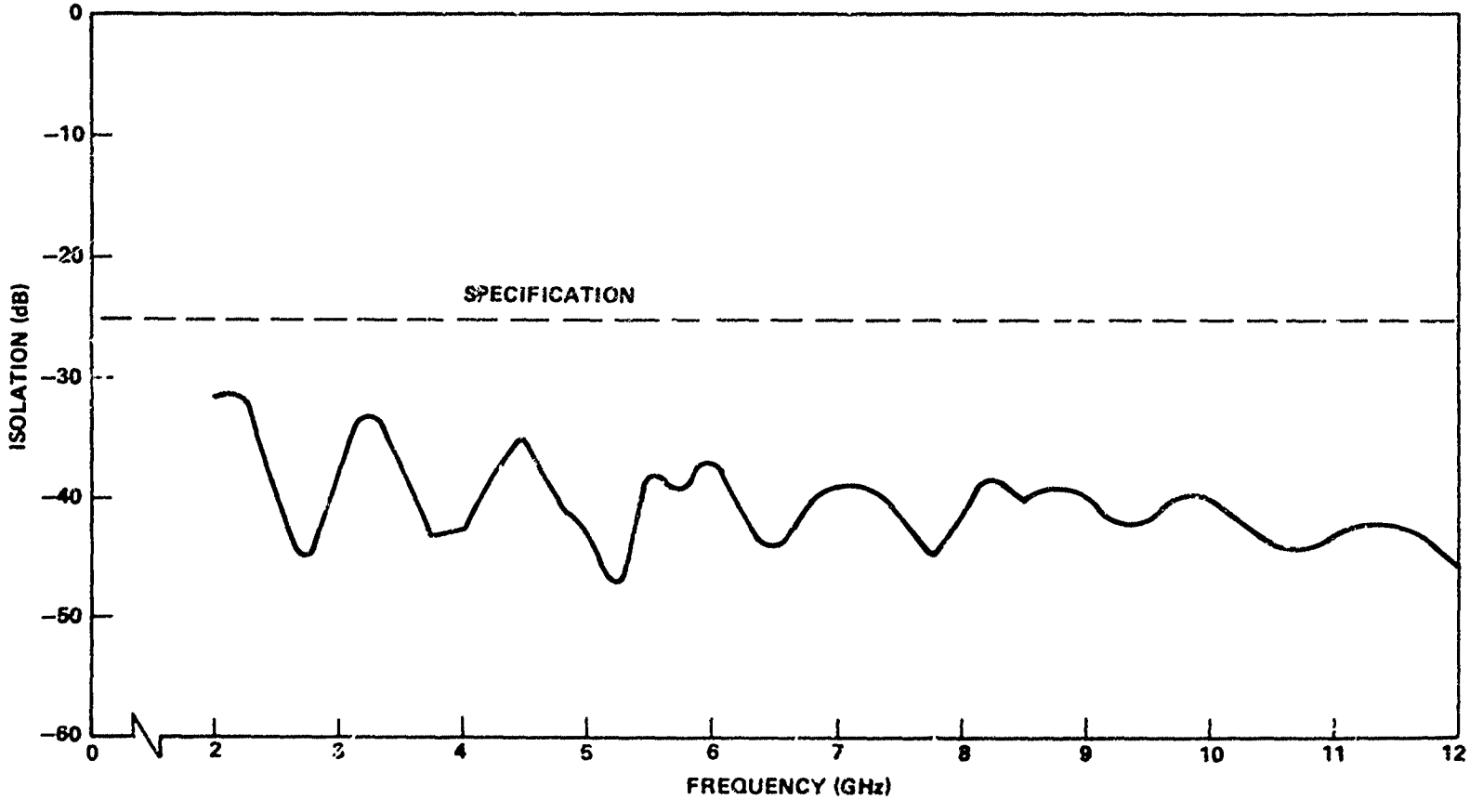

Figure 19. Isolation characteristics of MICOM horn.

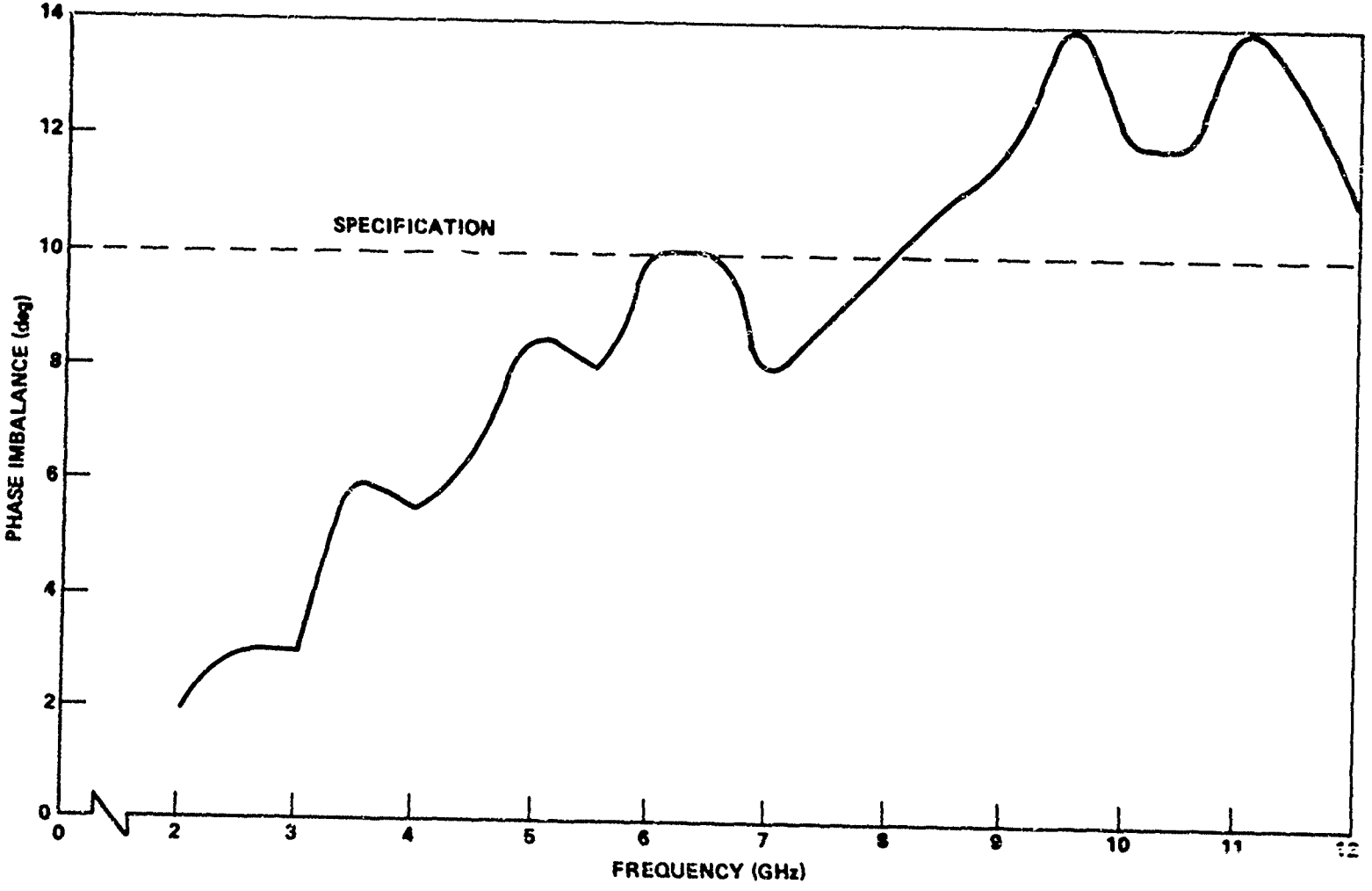

Figure 20. Phase imbalance between ports.

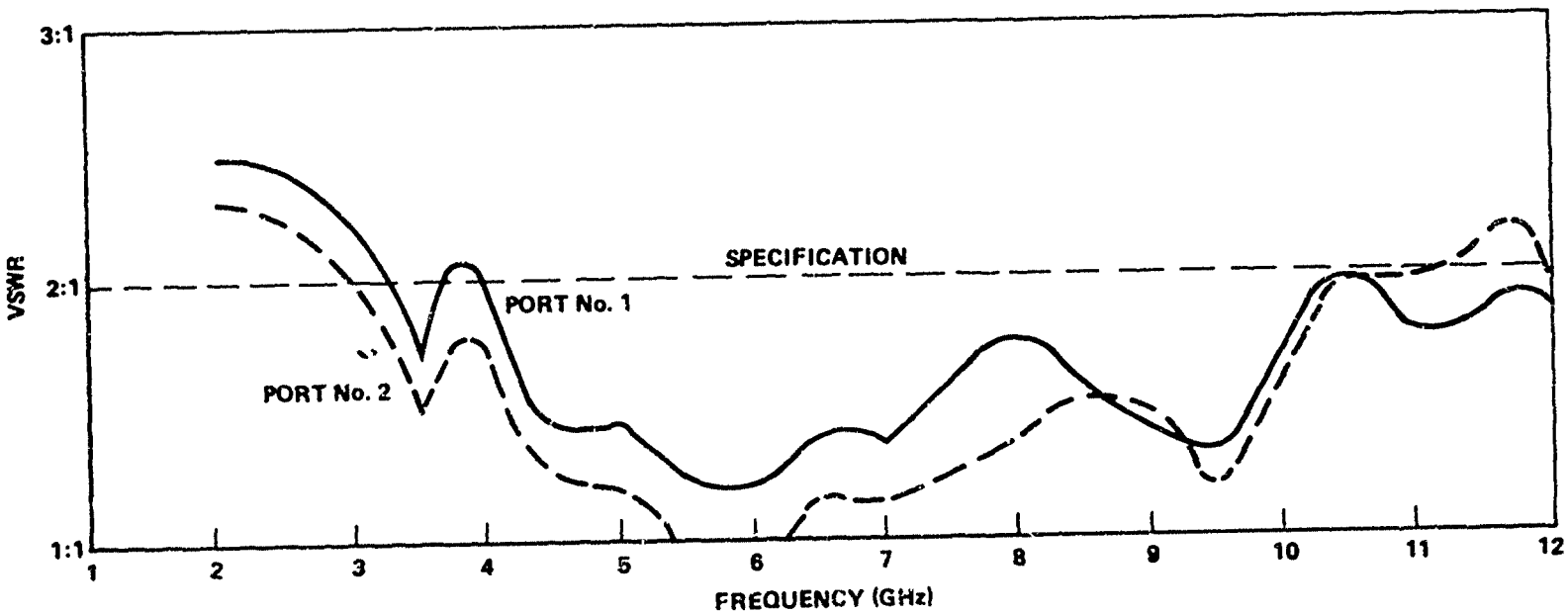

Figure 21. VSWR characteristics of MICOM horn. (Gap width 0.033 inch.)

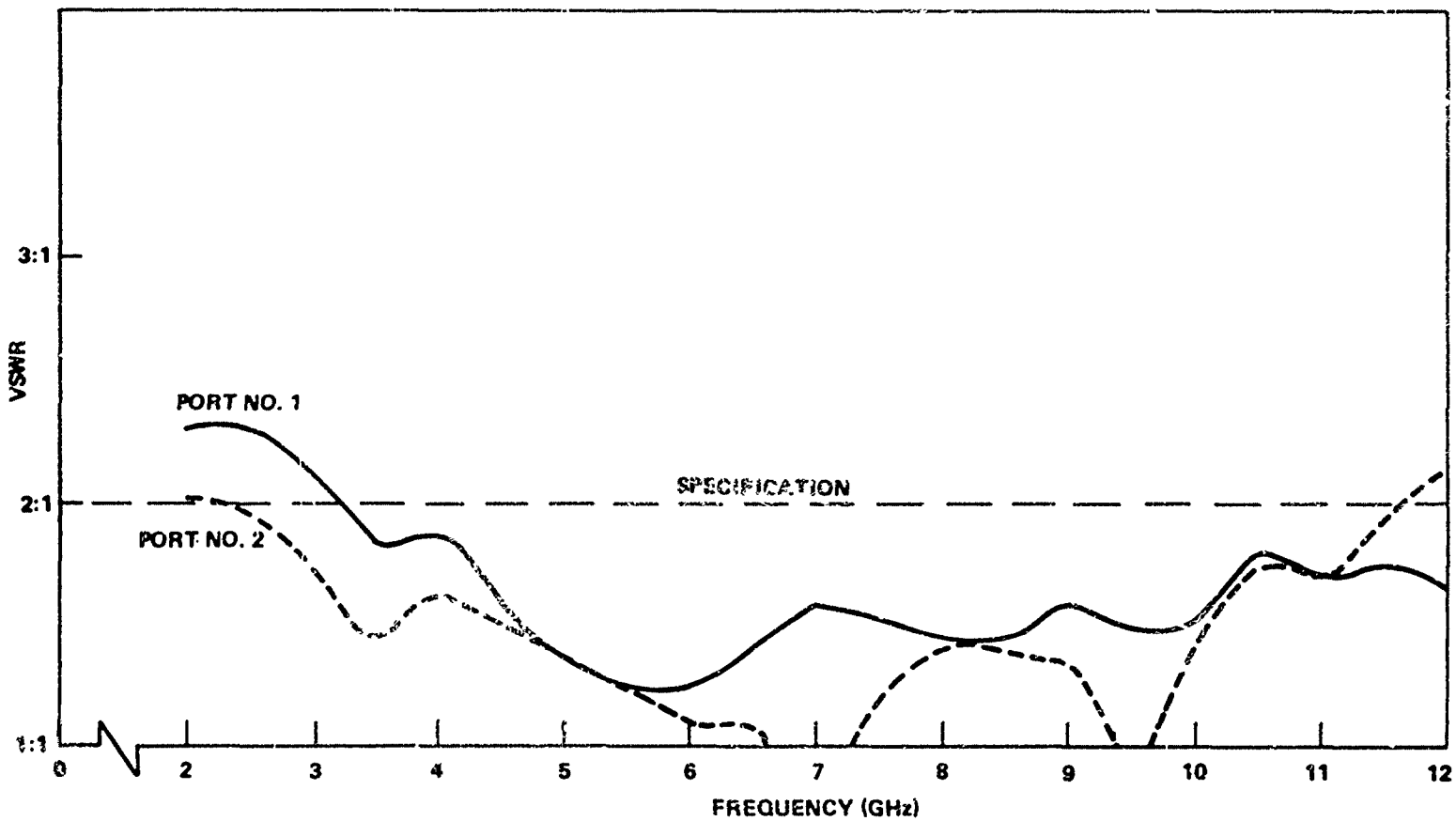

Figure 22. VSWR characteristics of MICOM horn. (Gap width 0.026 inch.)

All results previously discussed were for the MICOM-30 horn or the horn with the 0.030 inch probe separation. Results for the MICOM-20 horn or the horn with the 0.020 inch probe separation generally were slightly better in the VSWR and cross-polarization characteristics. Work on the design of the two MICOM horns were redirected from the 2 - 12 GHz frequency band to a broader frequency band of 2 - 18 GHz. Many specifications were relaxed with this redirection.

Section VII. CONCLUSIONS

This report presents the results of an investigation in the design of a broadband quadruple-ridged waveguide radiator. It covers the theoretical and practical aspects in the design of the ridged waveguide parameters, the design of the ridges in the flared section, and the design of the coaxial to ridged waveguide transformer.

The result of the investigation is a usable 2 - 12 GHz bandwidth, dual-polarization, quadruple-ridged horn which is an advancement in the state-of-the-art. It is felt that further refinement in the design of the two constructed engineering models would have corrected the marginal VSWR and cross-polarization characteristics at the extreme lower end of the frequency band. The difference in characteristics between the two horns can be attributed to construction differences and gives some indication as to what tolerance controls are needed in the production of a large number of antennae of this design.

REFERENCES

1. Cohn, Seymour B., "Properties of Ridged Wave Guide," Proc. IRE, Vol. 35, August 1947, pp. 783-788.

2. Whinnery, J. R. and Jamieson, H. W., "Equivalent Circuits for Discontinuities in Transmission Lines," Proc. IRE, Vol. 32, February 1944, pp. 98-116.

3. Hopfer, Samuel W., "The Design of Ridged Waveguides," IRE Trans. MTT, Vol. MTT-3, October 1955, pp. 20-29.

4. Marcuvitz, N., Waveguide Handbook, M.I.T. Rad. Lab. Ser., Vol. 10, N.Y.: McGraw-Hill, 1951, pp. 399-402.

5. Walton, K. L. and Sundberg, V. C., "Broadband Ridged Horn Design," Microwave J., March 1964, pp. 96-101.

6. Pyle, J. R., "The Cutoff Wavelength of the TE_{10} Mode in Ridged Rectangular Waveguide of Any Aspect Ratio," IEEE Trans. Microwave Theory Tech., Vol. MTT-14, April 1966, pp. 175-183.

7. Getsinger, W. J., "Ridged Waveguide Field Description and Application to Directional Couplers," IRE Trans. Microwave Theory Tech., Vol. MTT-10, January 1962, pp. 41-50.

8. Montgomery, James P., "On the Complete Eigenvalue Solution of Ridged Waveguide," IEEE Trans. Microwave Theory Tech., Vol. MTT-19, June 1971, pp. 547-555.

9. Sexson, T., Quadruply Ridged Horn, TR ECOM-0181-M1160, March 1968, Sylvania Electronic Defense Laboratories, DAAB07-67-C-0181.

10. Chen, C. C., Wong, N. S., and Tang, R., Ultra-Wideband Phased Arrays, Final Report AFCRL-TR-73-0569, July 1973, Hughes Aircraft Company, F19628-72-C-0224.

11. Chen, M. H. and Tsandoulas, G. N., "Bandwidth Properties of Quadruple-Ridged Circular and Square Waveguide Radiators," PGAP Symposium Record, August 1973.

12. Chen, M. H., Tsandoulas, G. N., and Willwerth, F. G., "Modal Characteristics of Quadruple-Ridged Circular and Square Waveguides," to be published in IEEE Trans. Microwave Theory Tech., Vol. MTT-12, August 1974.

13. Konrod, A., and Sylvester, P., "Scalar Finite-Element Program Package for Two-Dimensional Field Problems," IEEE Trans. Microwave Theory Tech., Vol. MTT-19, December 1971, pp. 962-954.

14. Kerr, John L., A Very Broad Band Low Silhouette Antenna, TR ECOM-3087, January 1969, US Army Electronics Command.

15. Kerr, John L., Short Axial Length Broadband Horns, TR ECOM-3344, October 1970, US Army Electronics Command.

16. Kerr, John L., Broadband Horns, TR ECOM-3319, August 1970, US Army Electronics Command.

17. Slater, J. C., Microwave Transmission, McGraw-Hill, New York, 1942, Chapter VII, pp. 280-304.

18. Ragan, George L., Microwave Transmission Circuits, M.I.T. Rad. Lab. Ser., Vol. 9, N.Y.: McGraw-Hill, 1948, pp. 314-361.

19. Cohn, Seymour B., "Design of Simple Broad-Band Wave-Guide-to-Coaxial-Line Junctions," Proc. IRE, Vol. 35, September 1947, pp. 920-926.

APPENDIX

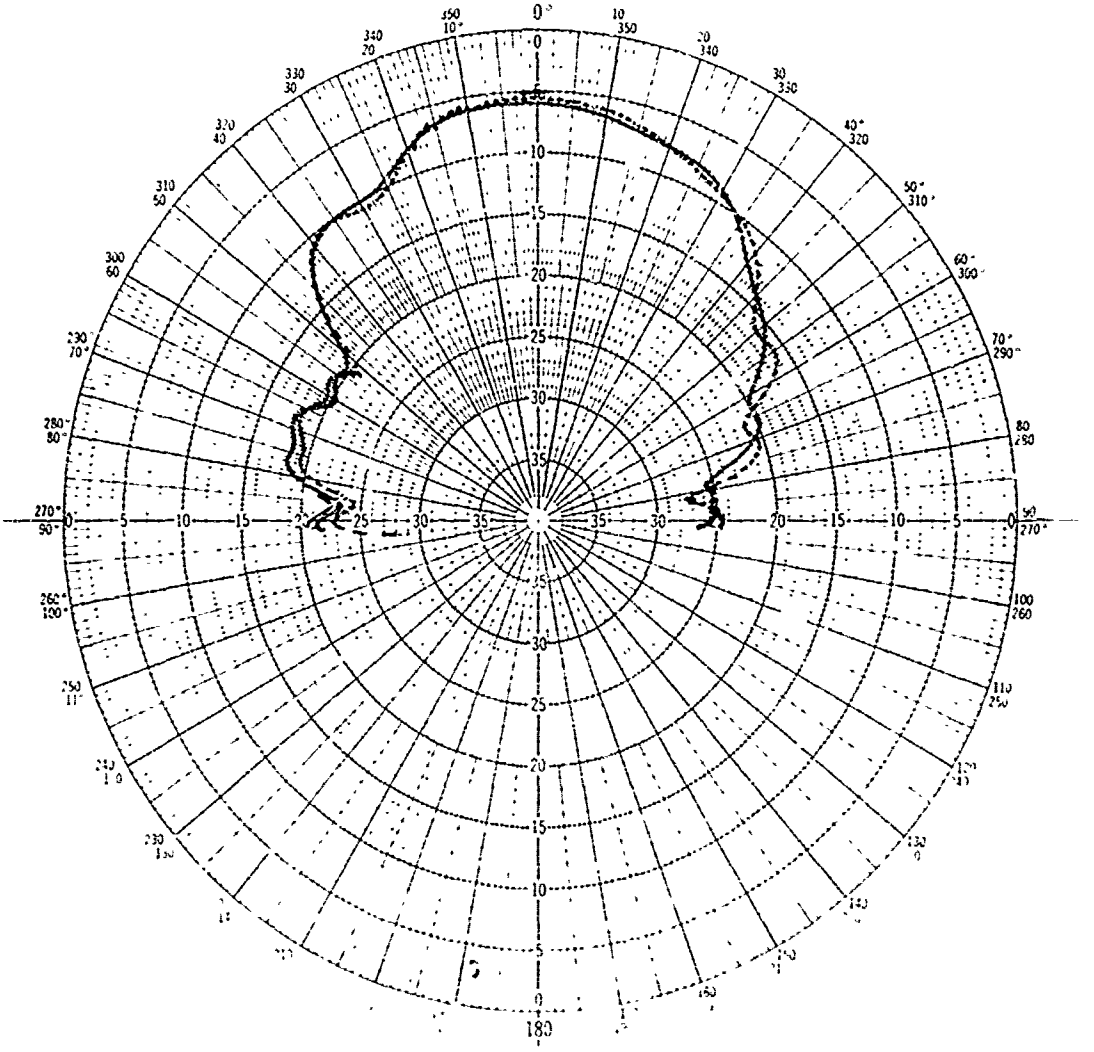

Figure A-1. E-plane patterns at 2 GHz (standard gain, 9.6 db).

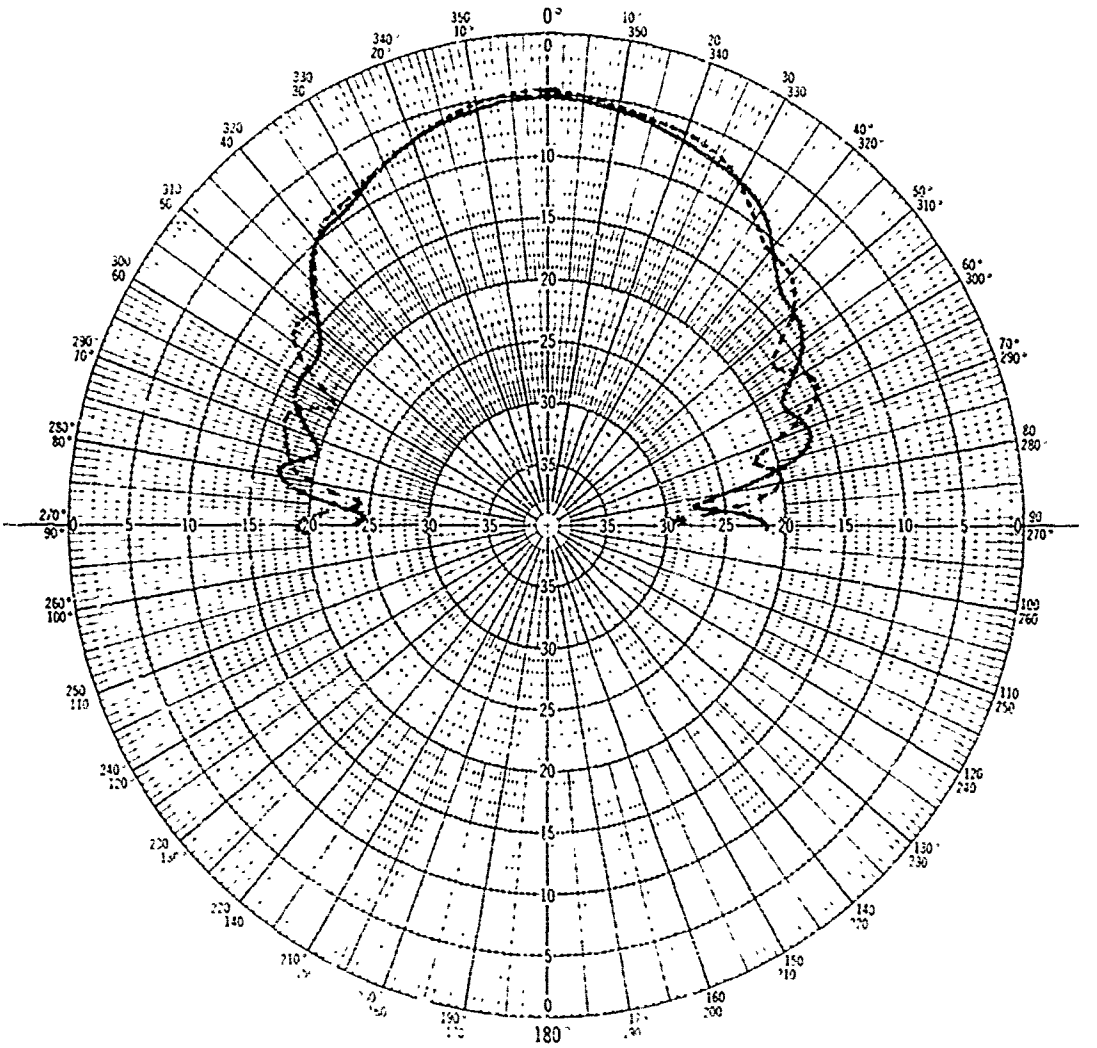

Figure A-2. H-plane patterns at 2 GHz (standard gain, 9.6 dB).

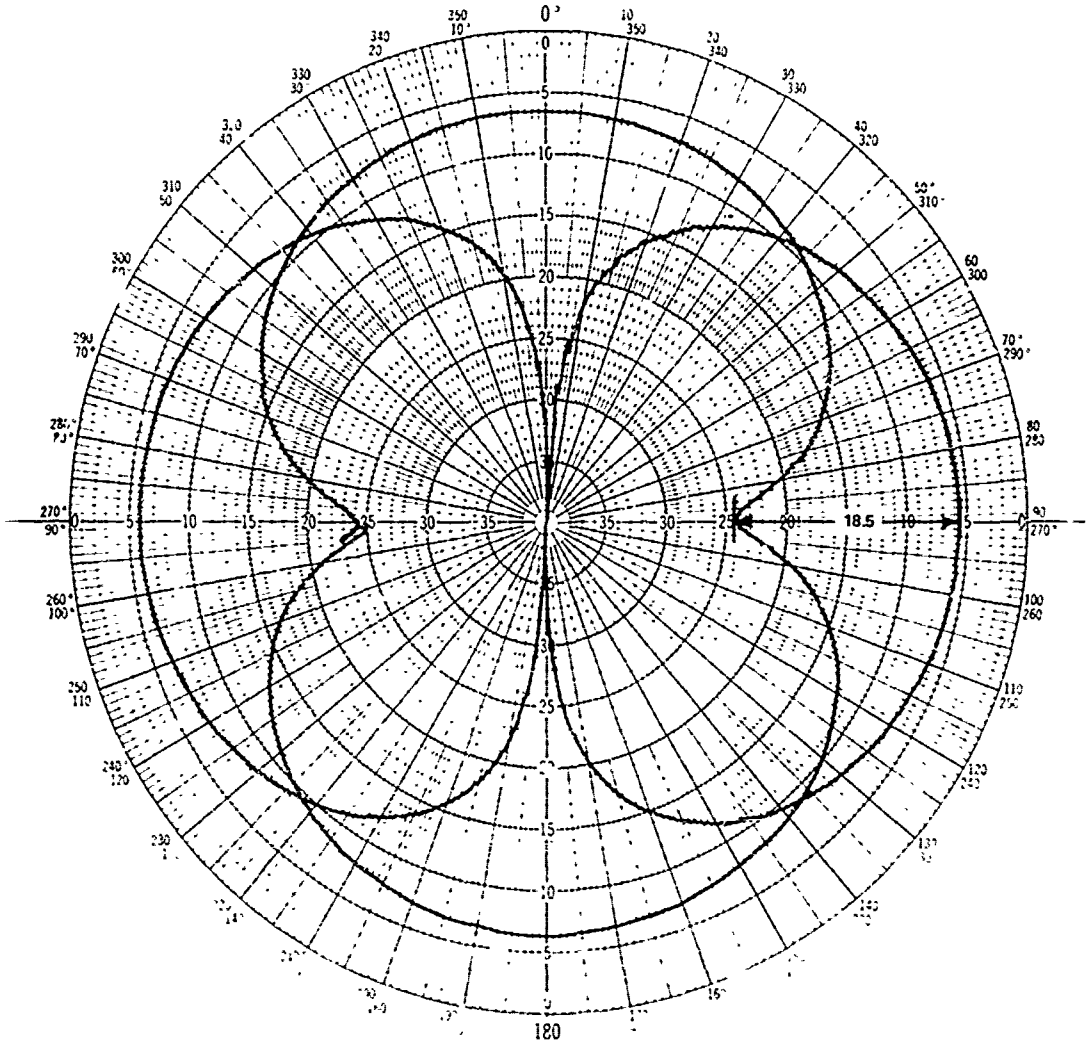

Figure A-3. On-axis-polarization patterns at 2 GHz (Top pattern is for Port 1 and other pattern is for Port 2).

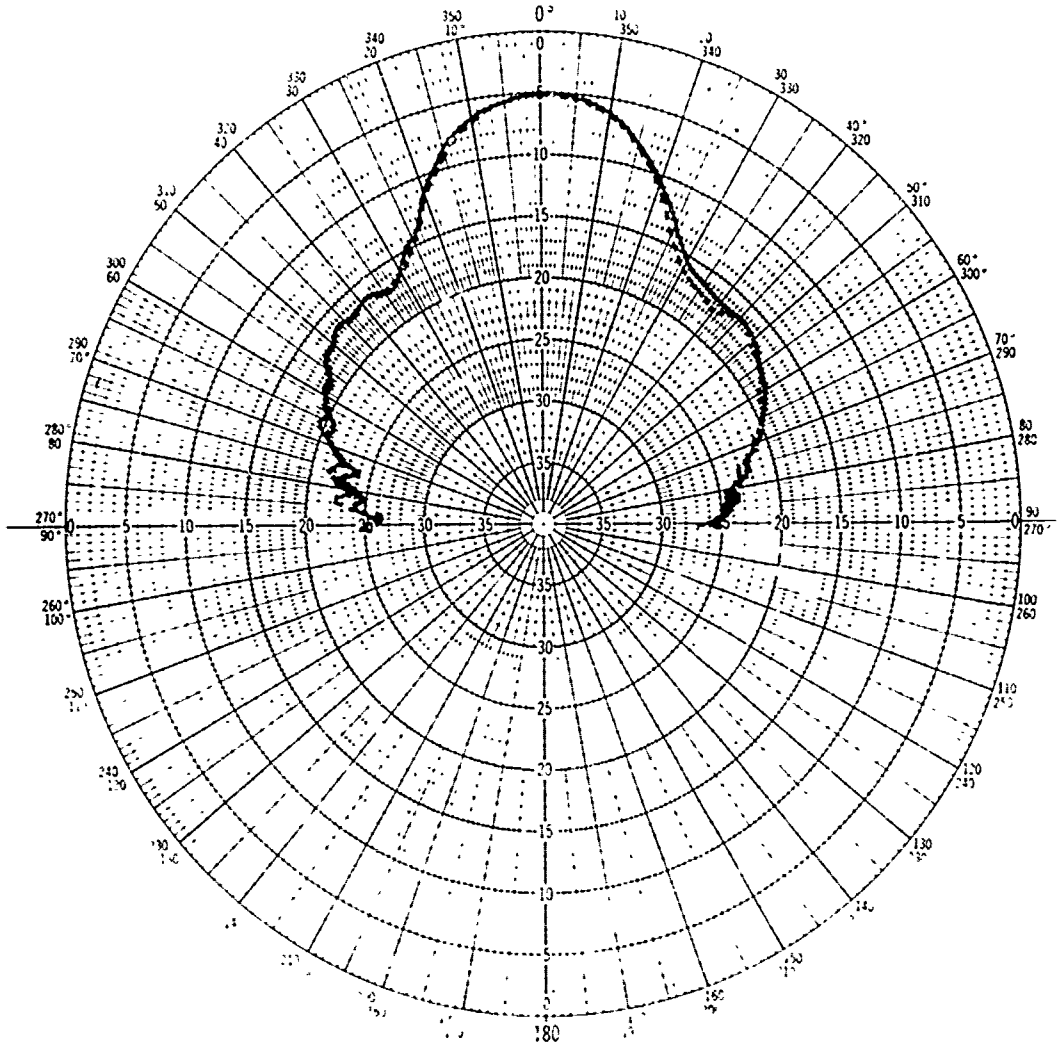

Figure A-4. E-plane patterns at 4 GHz (standard gain, 12 db).

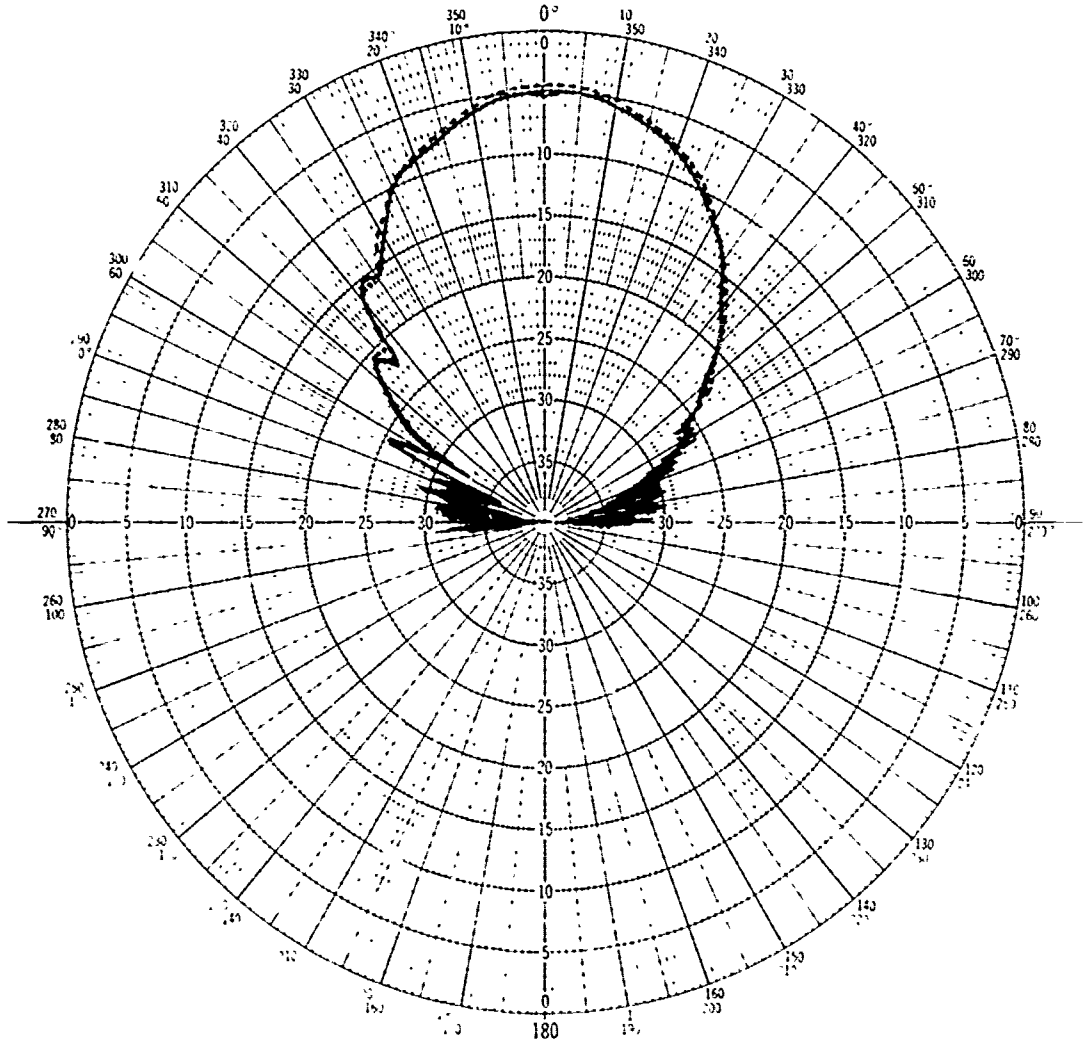

Figure A-5. H-plane patterns at 4 GHz (standard gain, 12 db).

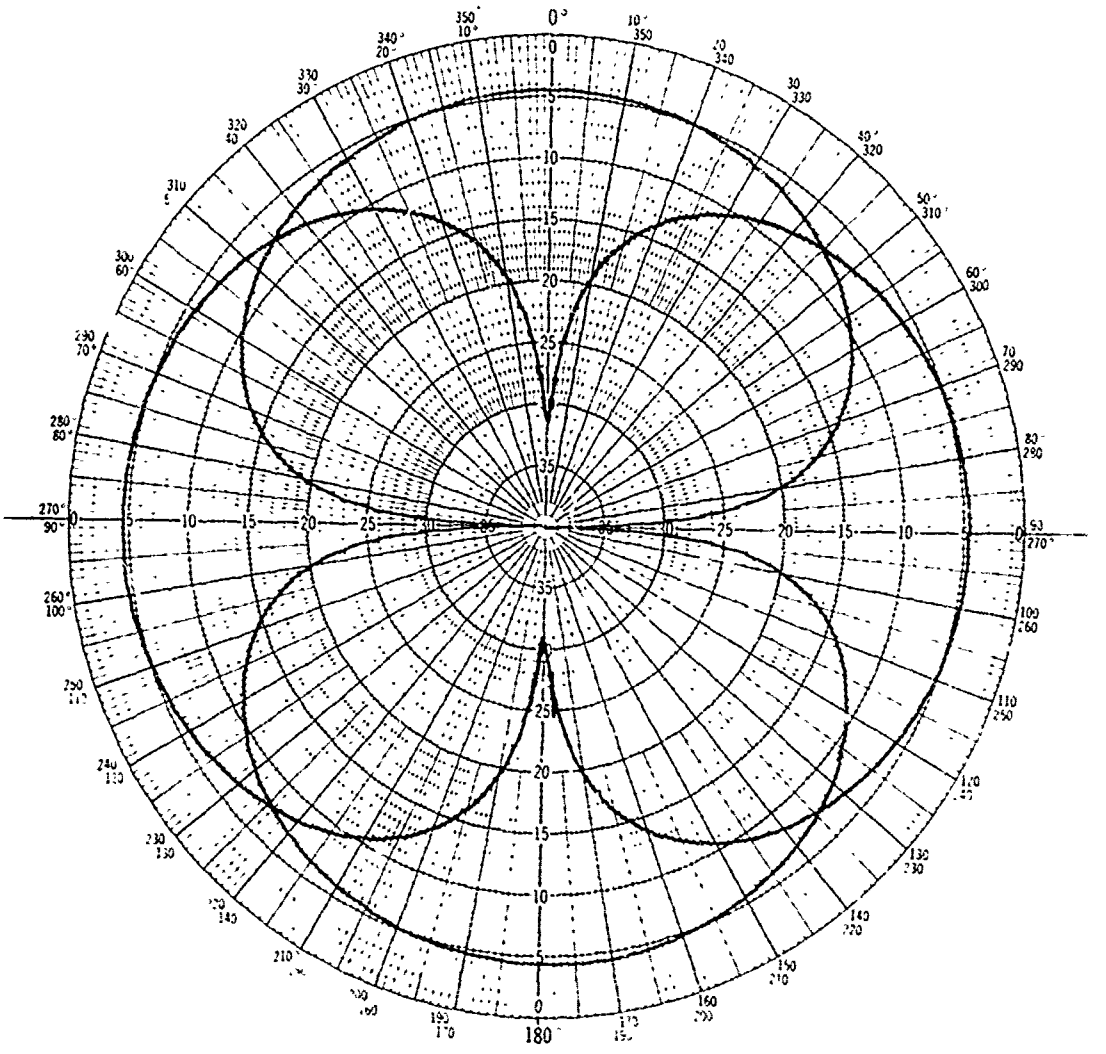

Figure A-6. On-axis-polarization patterns at 4 GHz (Top pattern is for Port 1).

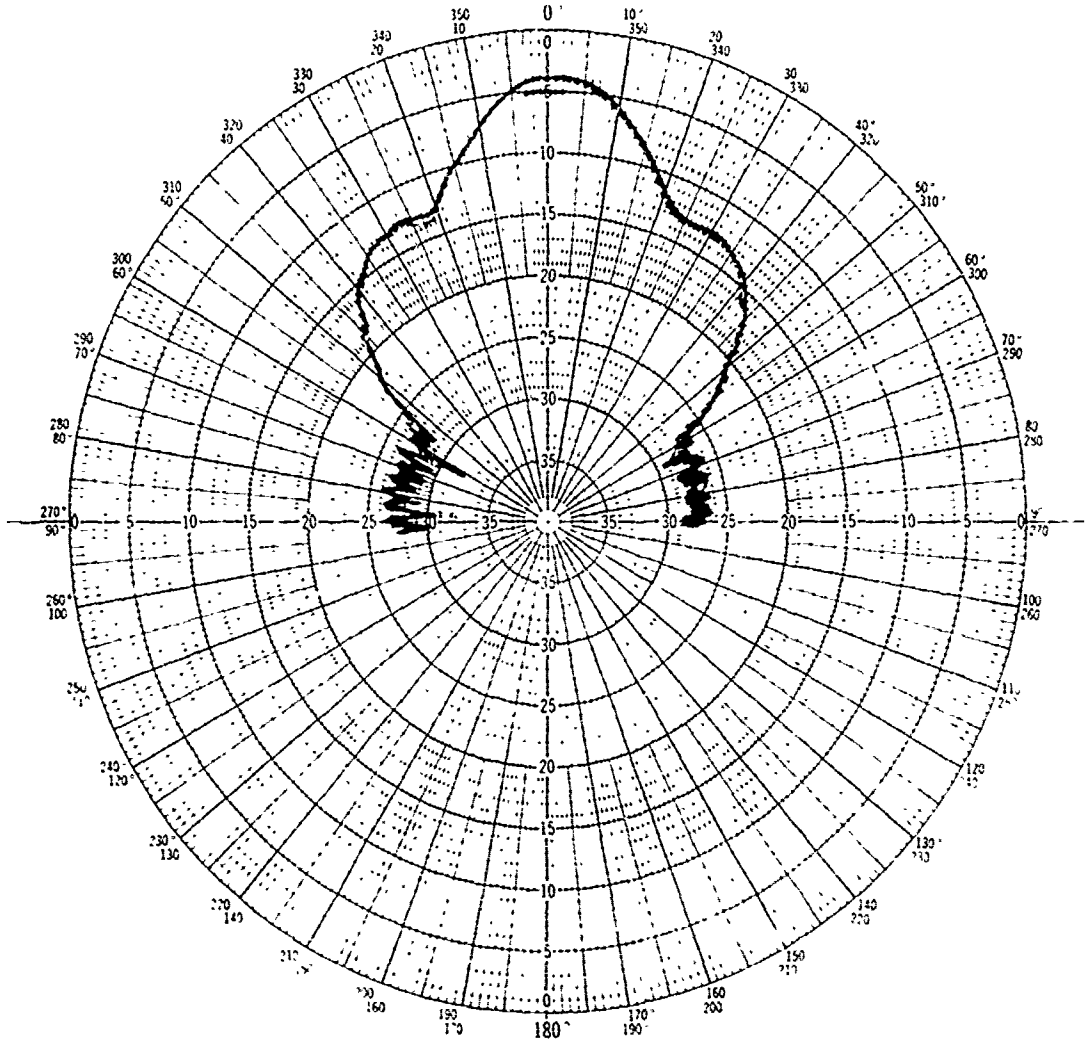

Figure A-7. E-plane patterns at 5.5 GHz (standard gain, 14 db).

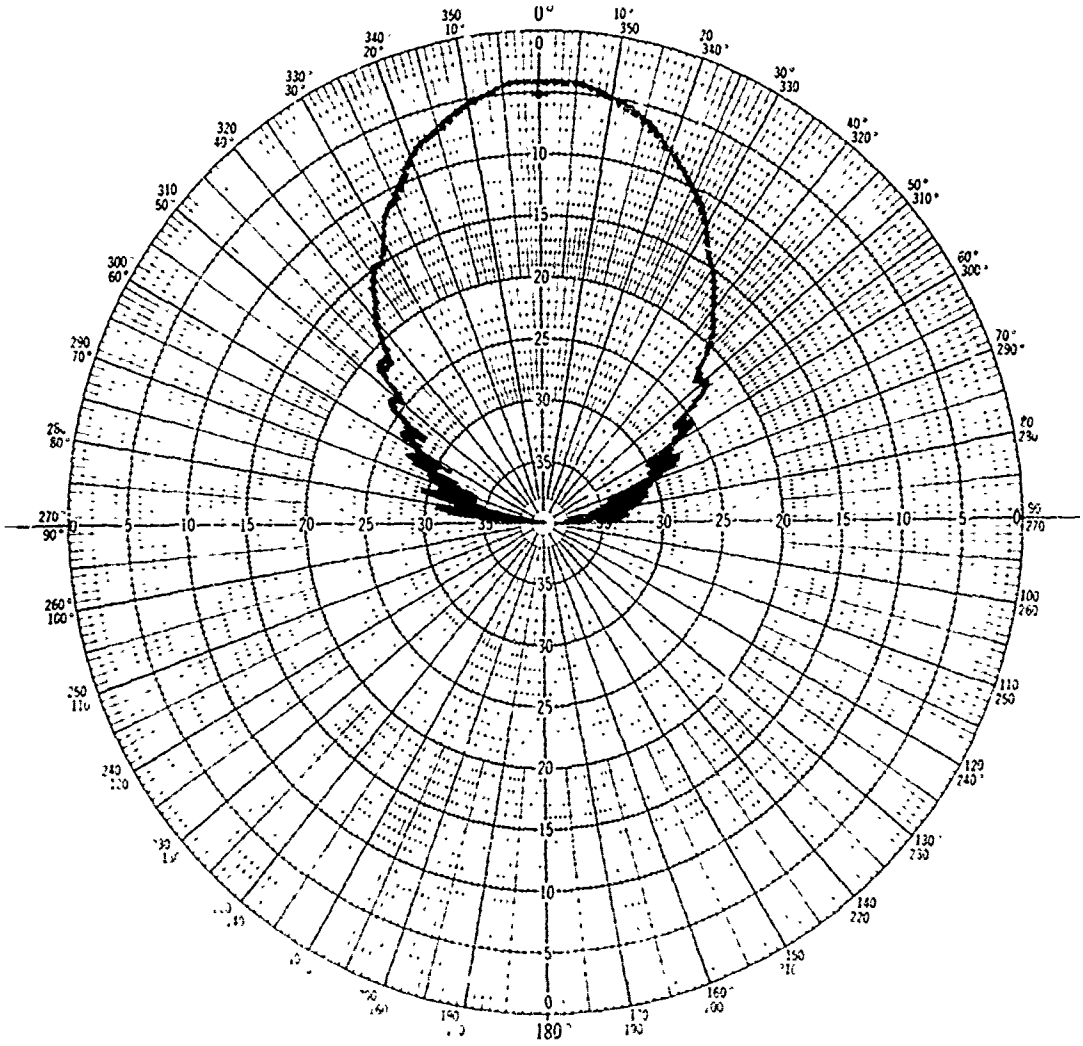

Figure A-8. H-plane patterns at 5.5 GHz (standard gain, 14 db).

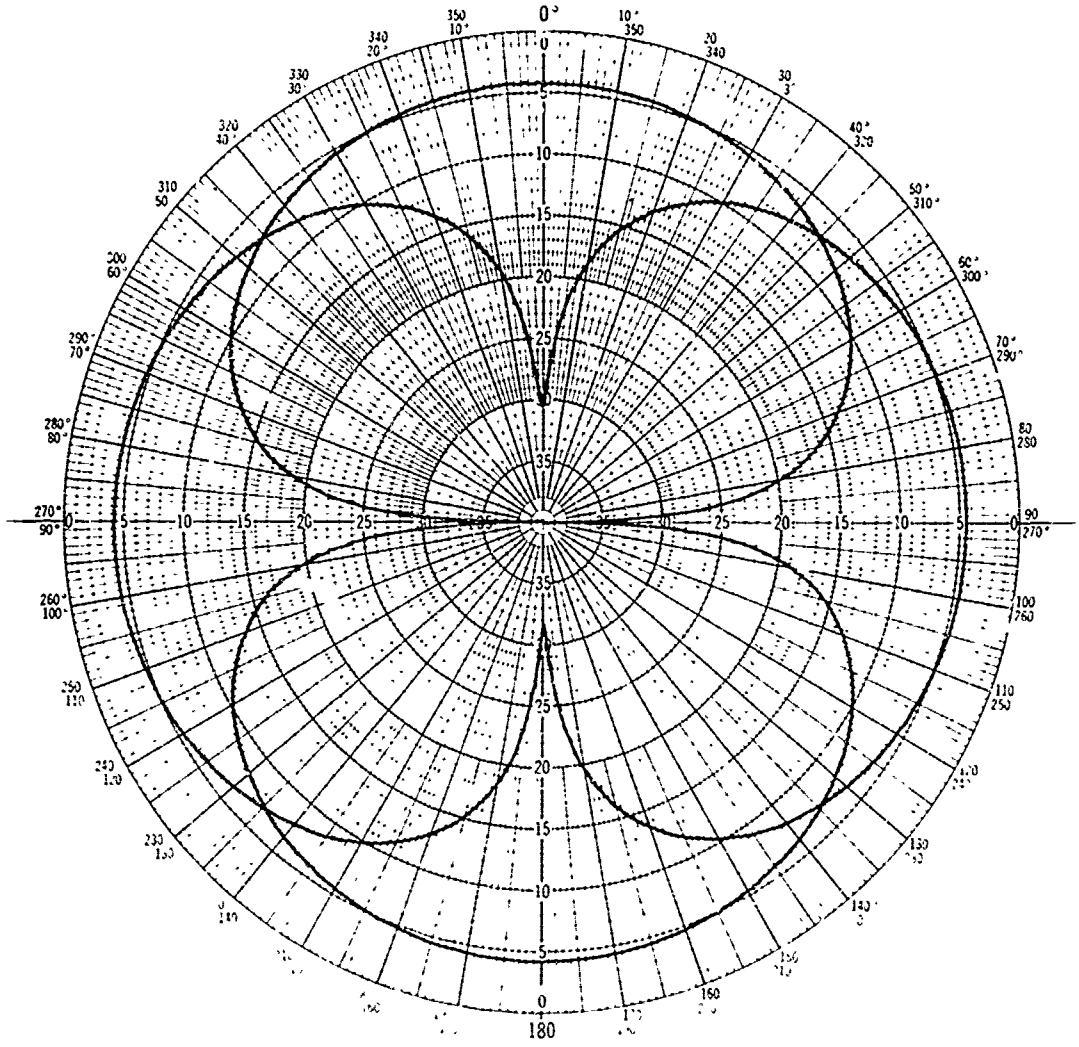

Figure A-9. On-axis-polarization patterns at 5.5 GHz (Top pattern is for Port 1).

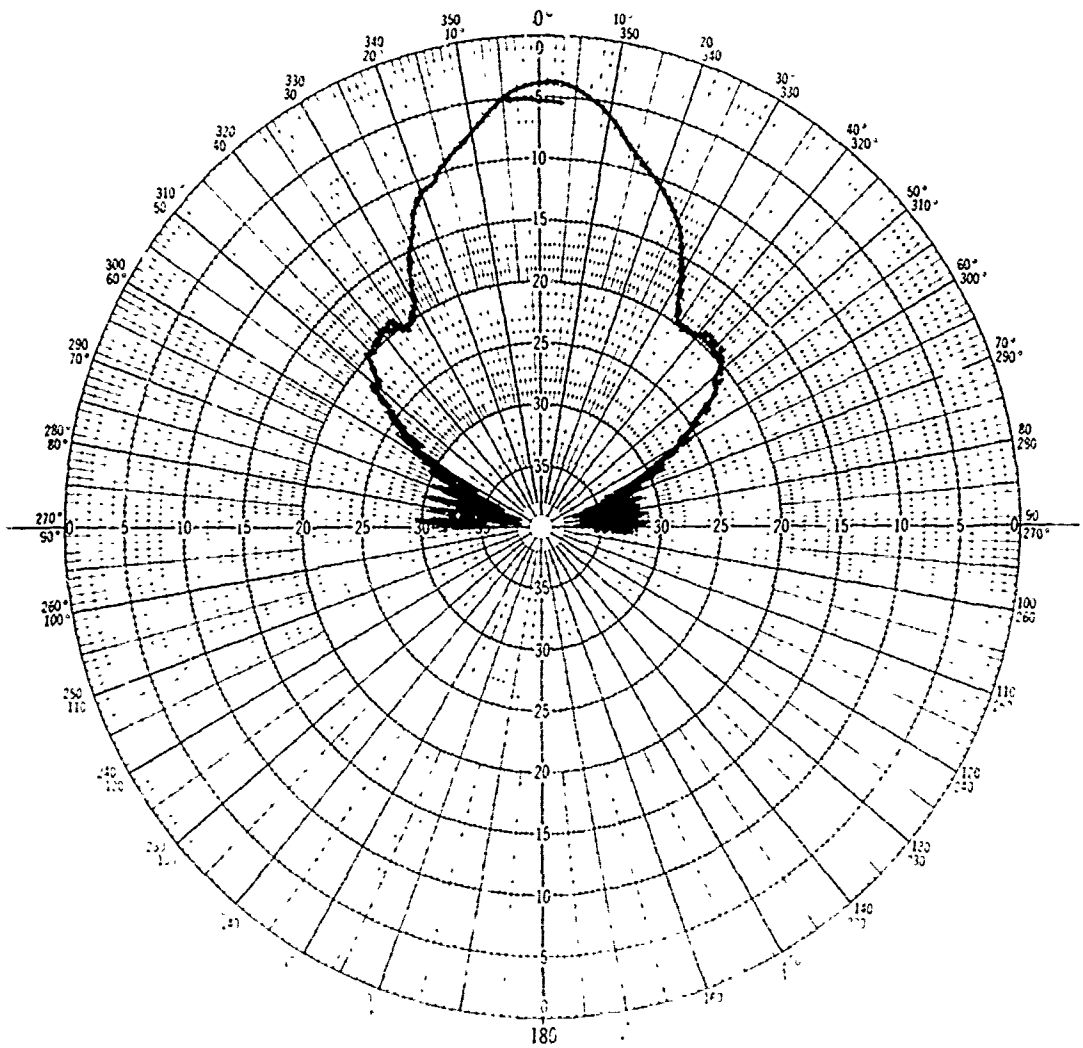

Figure A-10. E-plane patterns at 8 GHz (standard gain, 17 db).

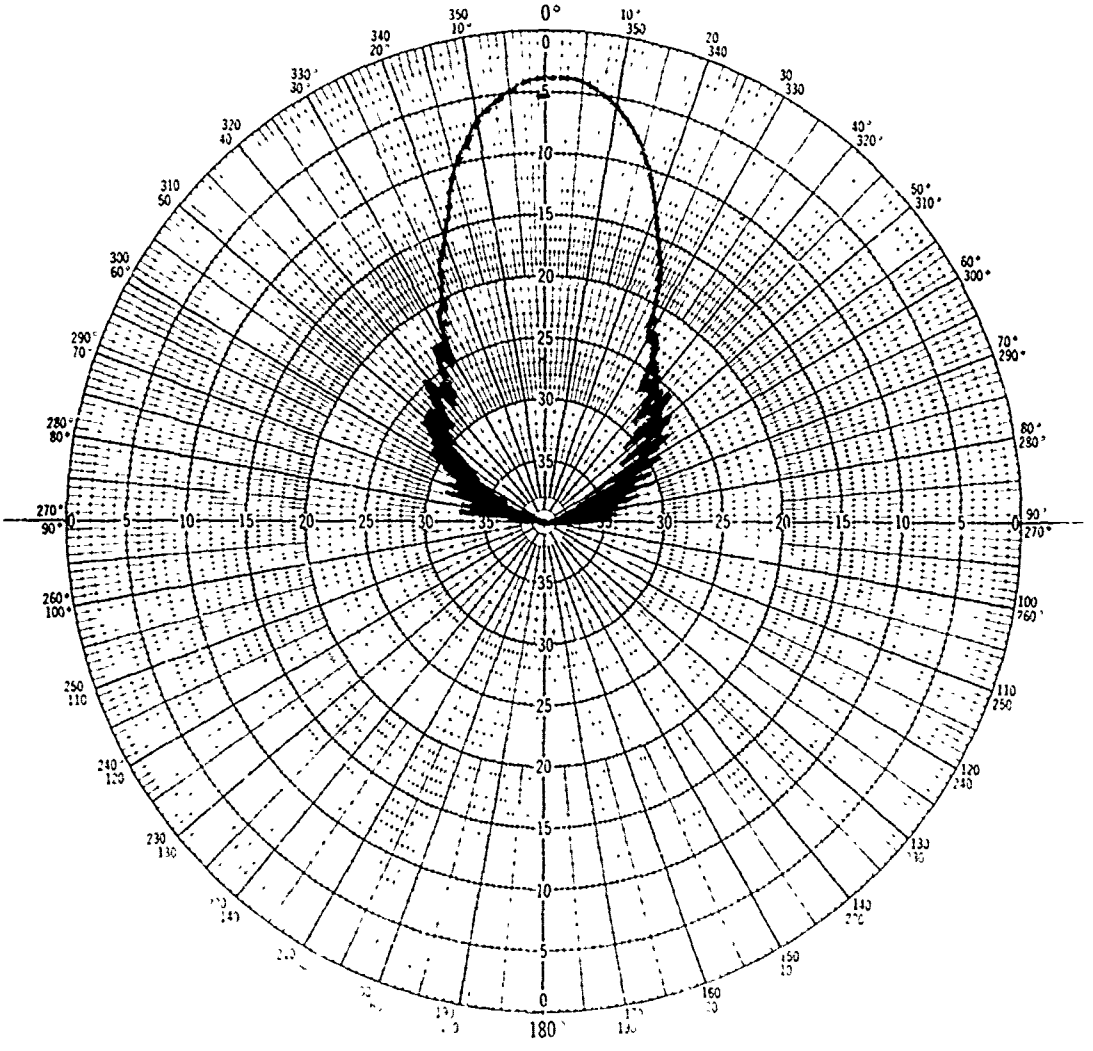

Figure A-11. H-plane patterns at 8 GHz (standard gai :b).

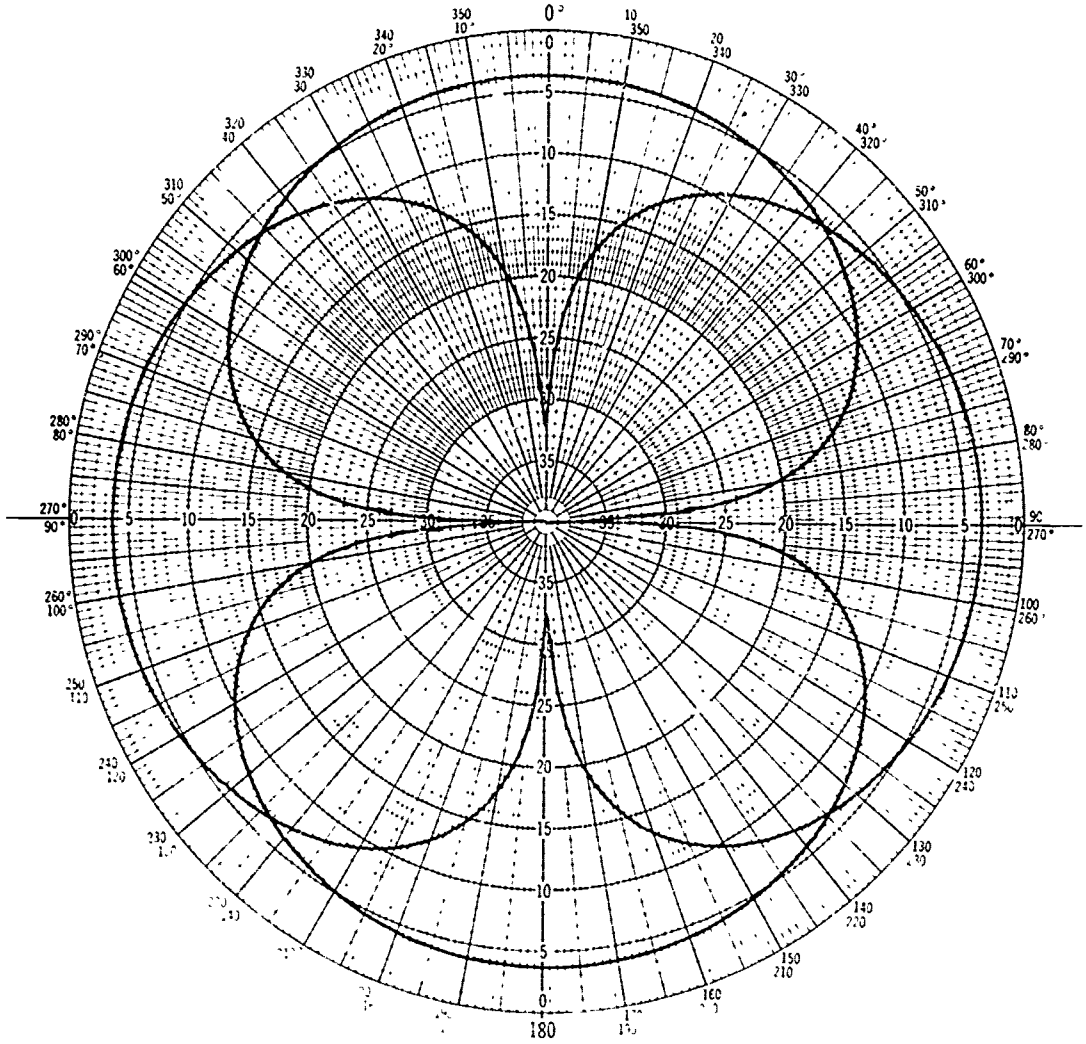

Figure A-12. On-axis-polarization patterns at 8 GHz (Top pattern is for Port 1).

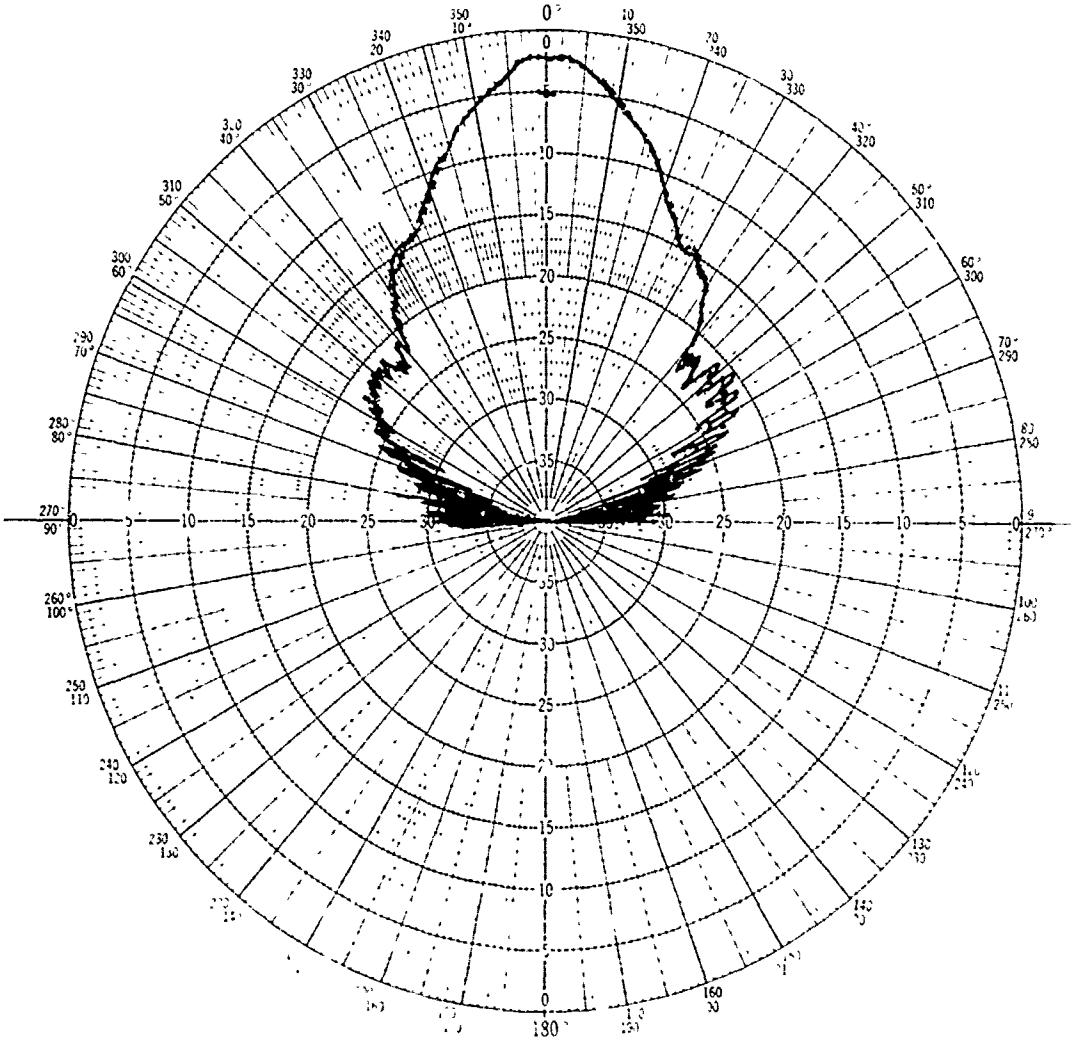

Figure A-13. E-plane patterns at 10 GHz (standard gain, 18.5 db).

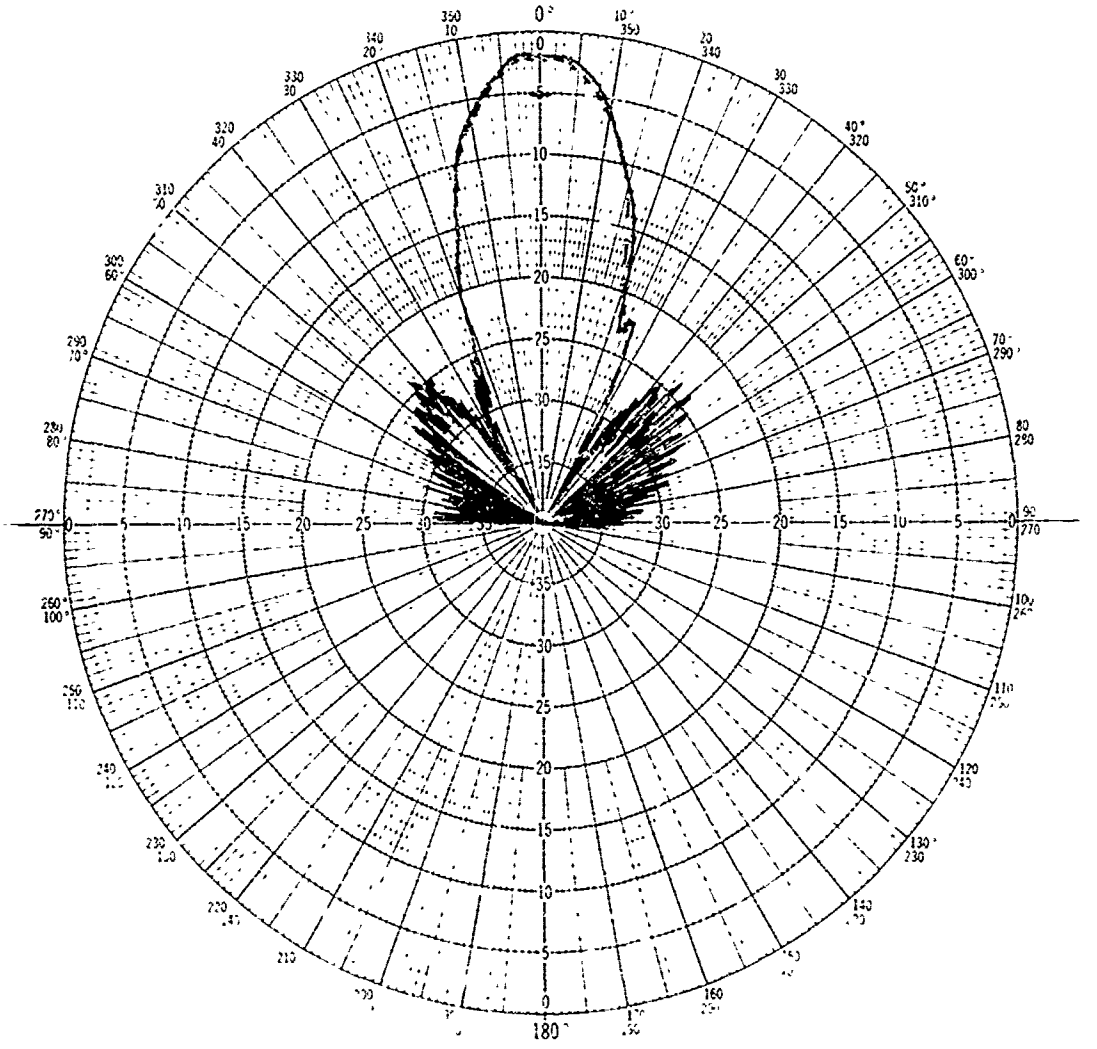

Figure A-14. H-plane patterns at 10 GHz (standard gain, 18.5 db).

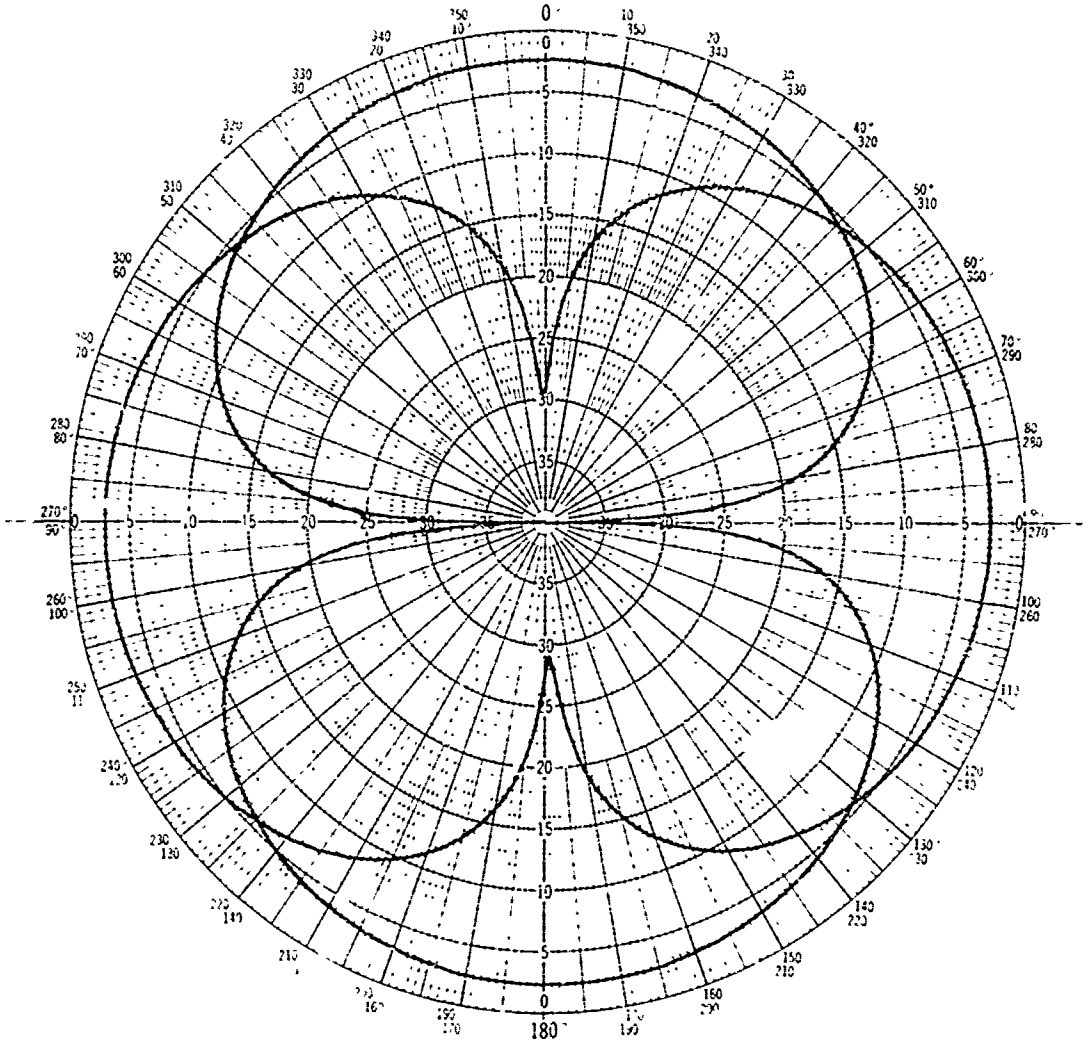

Figure A-15. On-axis-polarization patterns at 10 GHz (Top pattern is for Port 1).

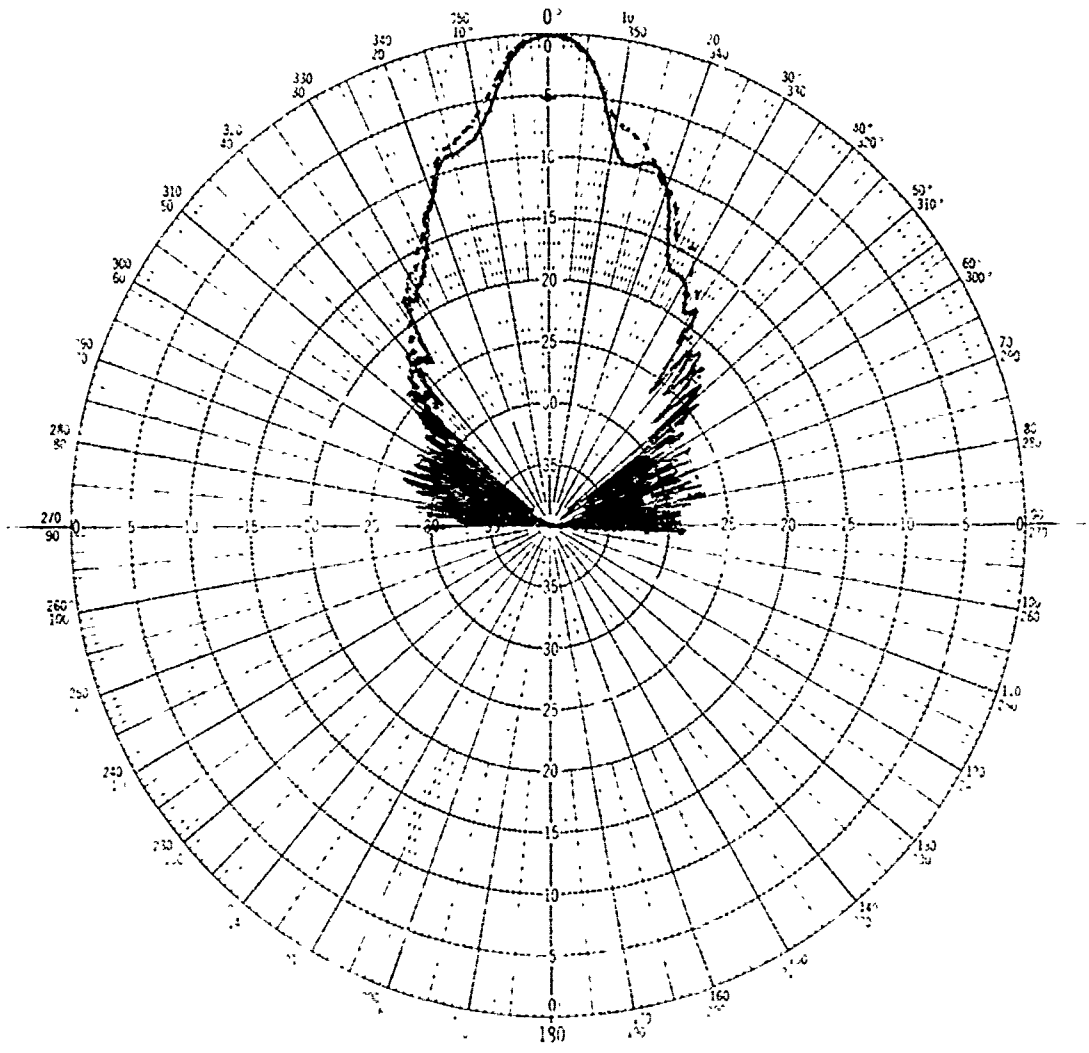

Figure A-16. E-plane patterns at 12 GHz (standard gain, 18 db).

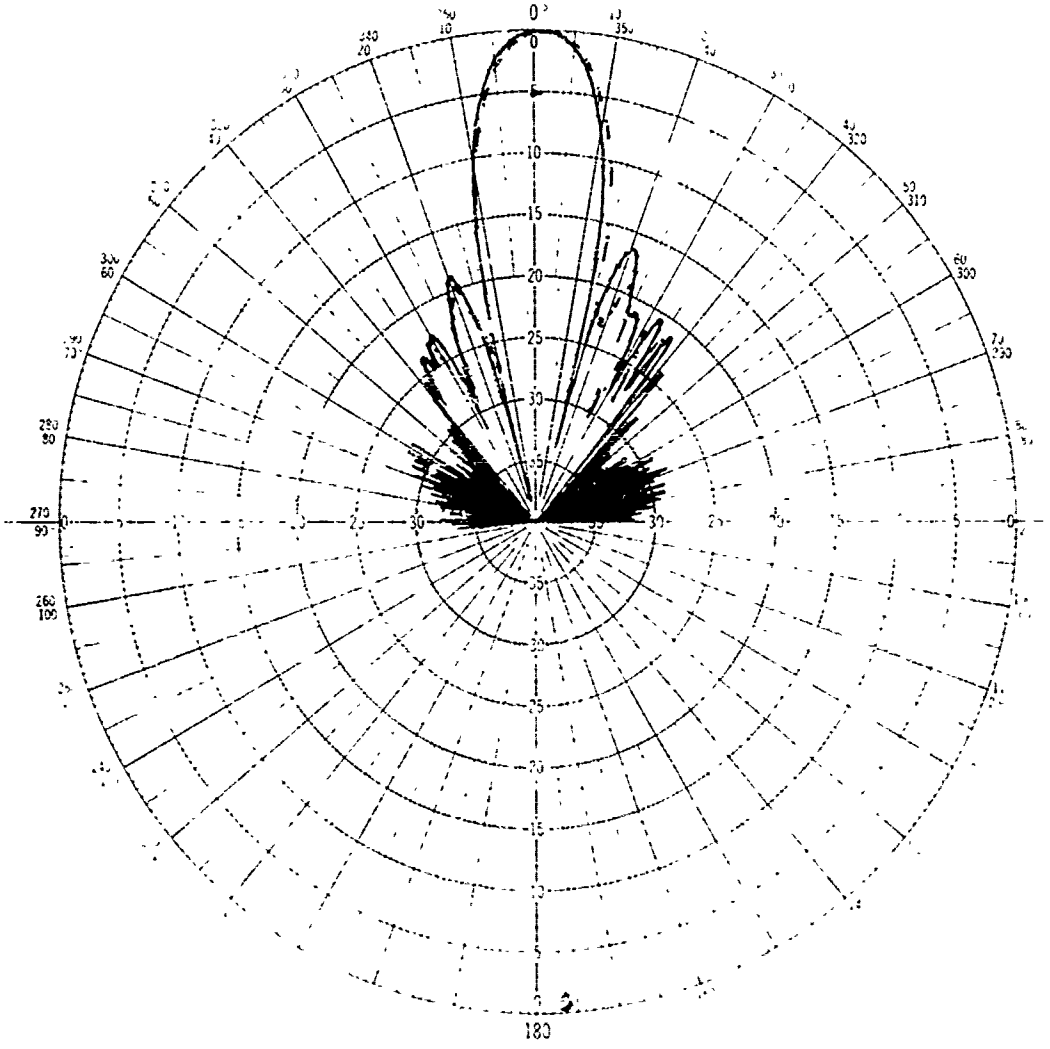

Figure A-17. H-plane patterns at 12 GHz (standard gain, 18 db).

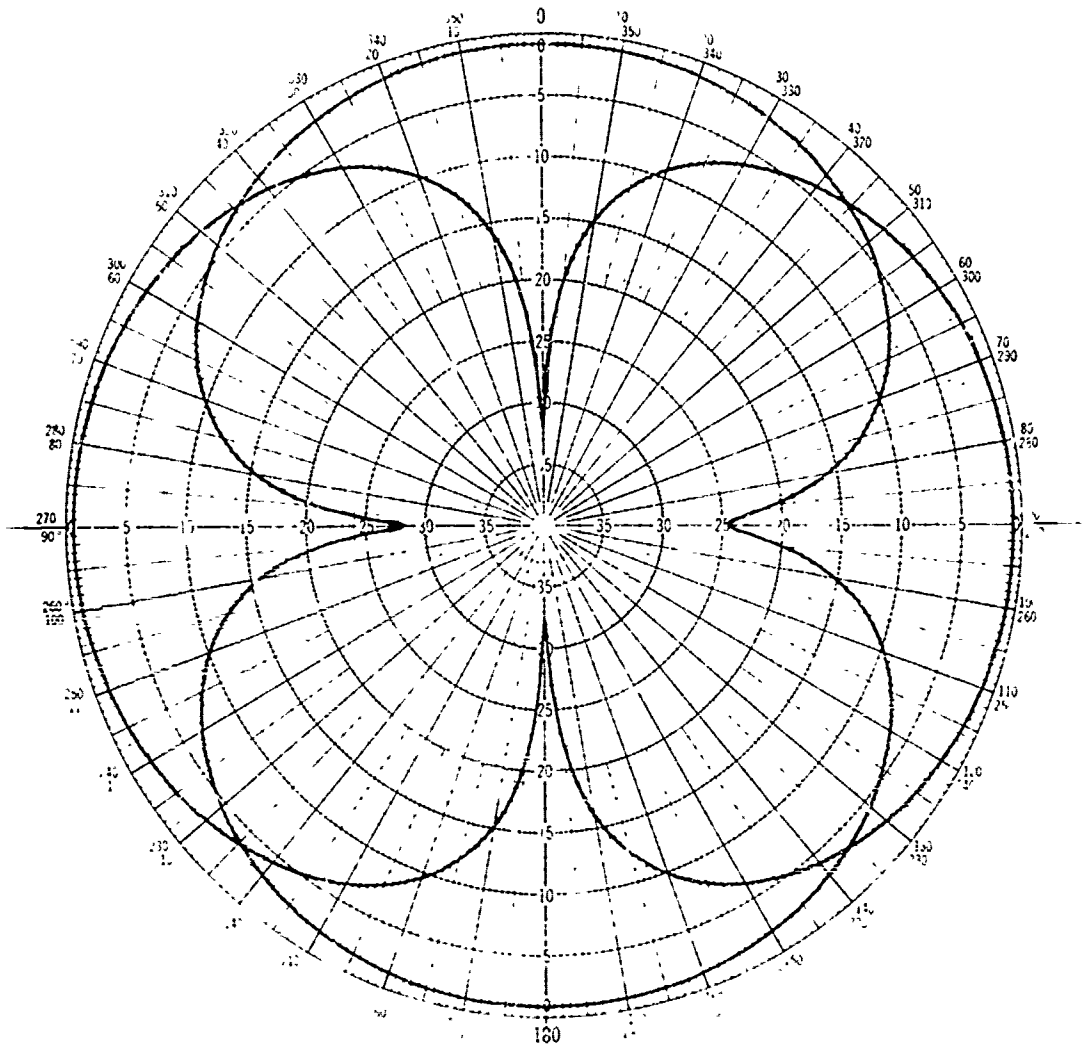

Figure A-18. On-axis polarization patterns at 12 GHz (Top pattern is for Port 1).